

1 **The cIAP ubiquitin ligases sustain type 3  $\gamma\delta$  T and innate lymphoid cells during**  
2 **aging to allow normal cutaneous and mucosal responses**

3 John Rizk<sup>1</sup>, Urs M. Mörbe<sup>1</sup>, Rasmus Agerholm<sup>1</sup>, Isabel Ulmert<sup>1</sup>, Elisa Catafal Tardos<sup>1</sup>,  
4 Darshana Kadekar<sup>1</sup>, Maria V. Baglioni<sup>1</sup>, Monica Torrellas Viñals<sup>1</sup> and Vasileios  
5 Bekiaris<sup>\*1</sup>

6 <sup>1</sup>Department of Health Technology, Technical University of Denmark, Kemitorvet, Bldg  
7 202, 2800 Kgs Lyngby, Denmark.

8 \*Corresponding author: Vasileios Bekiaris [vasbek@dtu.dk](mailto:vasbek@dtu.dk)

9

10 **Abstract**

11 Environmental and molecular cues early in life are often associated with the permanent  
12 shaping of our immune system during adulthood. Although increasing, our knowledge of  
13 the signaling pathways that operate in early life and their temporal mode of action is  
14 limited. Herein, we demonstrate that the cellular inhibitor of apoptosis proteins 1 and 2  
15 (cIAP1/2), which are E3 ubiquitin ligases and master regulators of the nuclear factor-  
16 kappa B (NF- $\kappa$ B) pathway, function during late neonatal and prepubescent life to sustain  
17 interleukin(IL)-17-producing gamma delta T cells ( $\gamma\delta$ T17) and group 3 innate lymphoid  
18 cells (ILC3). We show that cell-intrinsic deficiency in cIAP1/2 at 3-4 weeks of life leads  
19 to downregulation of the transcription factors cMAF and ROR $\gamma$ t, and failure to enter  
20 cytokine-induced cell cycle. This is followed by progressive loss of  $\gamma\delta$ T17 cells and ILC3  
21 while mice are aging. Mice deficient in cIAP1/2 have severely reduced  $\gamma\delta$ T17 cells and  
22 ILC3, present with suboptimal  $\gamma\delta$ T17 responses in the skin, lack small intestinal isolated  
23 lymphoid follicles and cannot control intestinal bacterial infection. Mechanistically, these  
24 effects appear to be dependent on overt activation of the non-canonical NF- $\kappa$ B pathway.

25 Our data identify the cIAP E3 ubiquitin ligases as critical early life molecular switches for  
26 establishing effective type-3 immunity during aging.

27

28

29 **Introduction**

30 The neonatal period is the time when our immune system is imprinted with life-long  
31 functional characteristics that maintain immunity to infection and prevent autoimmune  
32 pathology. Microbial colonization, and developmentally regulated transcriptional  
33 programs cooperate to shape innate and adaptive lymphocytes into distinct specialized  
34 lineages that co-exist in equilibrium and respond ad hoc (Eberl, 2016). Failure to convey  
35 these environmental and molecular cues during neonatal life, often results in irreversible  
36 dysfunction later on. Hence, early dysbiosis impairs type-3 immunity and potentiates  
37 susceptibility to type-2 driven allergy (Cahenzli *et al*, 2013) . Similarly, blockade of key  
38 signaling pathways during neonatal life can permanently change cellular niches  
39 (Kadekar *et al*, 2020). Therefore, elucidating the molecular signatures that operate early  
40 in life is of great importance for understanding how immunity develops.

41 Mouse  $\gamma\delta$  T cells present a well-established example of an immune population that  
42 is heavily dependent on an unperturbed neonatal period. In this regard, intestinal  
43 intraepithelial (IE)  $\gamma\delta$  T cells develop during neonatal and prepubescent life through  
44 butyrophylin-driven interactions with the epithelia (Di Marco Barros *et al*, 2016) . This  
45 provides a necessary defense mechanism against infection within the IEL compartment  
46 (Hoytema van Konijnenburg *et al*, 2017). Lamina propria (LP) interleukin(IL)-17-  
47 producing  $\gamma\delta$  T cells establish mixed type-3 and type-1 transcriptional programs within  
48 the first week of life through the transcription factor STAT5 (Kadekar *et al*, 2020) . Thus,

49 early life establishment of the  $\gamma\delta$ T17 compartment is critical to protect from neonatal  
50 and adult infections (Chen *et al*, 2020; Sheridan *et al*, 2013). In a similar manner,  
51 impaired microbial colonization of the ocular or oral mucosa results in drastically altered  
52 IL-17-producing  $\gamma\delta$  T ( $\gamma\delta$ T17) cell numbers in the conjunctiva (St. Leger *et al*, 2017) and  
53 cervical lymph nodes (LN) (Fleming *et al*, 2017). Again, paucity in such  $\gamma\delta$ T17 cell  
54 populations is associated with impaired anti-microbial responses in eye and oral cavity  
55 (Conti *et al*, 2014; St. Leger *et al*, 2017), and resistance to pathogenic inflammation (Cai  
56 *et al*, 2011; Sandrock *et al*, 2018; McGinley *et al*, 2020).

57 The innate lymphoid cell (ILC) compartment is also dependent on early life events,  
58 while their function during the neonatal period is critical for the establishment of the  
59 intestinal immune system (Spits *et al*, 2013). In this regard, although dysbiosis does not  
60 affect ILC development, it results in altered transcriptional and epigenetic profiles of all  
61 ILC subsets (Gury-BenAri *et al*, 2016). Similar to LP  $\gamma\delta$ T17 cells, group 3 ILC (ILC3)  
62 acquire expression of the transcription factor Tbet and the type-1 cytokine interferon- $\gamma$   
63 (IFN- $\gamma$ ) during neonatal life, which allows them to clear intracellular bacterial infections  
64 (Klose *et al*, 2013) . Moreover, group 2 ILC (ILC2) undergo an IL-33-dependent  
65 maturation step in the neonatal lung, allowing their cytokine responsiveness in adult  
66 mice (Steer *et al*, 2020). Importantly, ILC3 induce the maturation of intestinal  
67 cryptopathces into isolated lymphoid follicles (ILFs) during the first 3-4 weeks of life  
68 (Kiss *et al*, 2011; Kruglov *et al*, 2013). Evidently, perturbations of  $\gamma\delta$ T17 and ILC3  
69 development during the early stages of life will have a substantial impact on the quality  
70 of immunity while aging. The molecular pathways that control the transition of these  
71 cells from neonatal life to adolescence and adulthood are poorly understood.

72 The E3 ubiquitin ligases cellular inhibitor of apoptosis protein (cIAP)1 and 2  
73 (cIAP1/2) catalyze both degradative lysine(K)-48 and stabilizing K-63 ubiquitination and  
74 act as the main molecular switches for the activation of the canonical and non-canonical  
75 nuclear factor-kappa B (NF- $\kappa$ B) pathway (Silke & Meier, 2013) . The presence of  
76 cIAP1/2 downstream of TNF receptor 1 (TNFR1) determines whether a cell will initiate  
77 the canonical NF- $\kappa$ B pathway or die by apoptosis or necroptosis in response to TNF  
78 (Annibaldi & Meier, 2018). They achieve this by ubiquitinating receptor interacting  
79 kinase-1 (RIPK1) (Silke & Meier, 2013) . However, cIAP1/2 are mostly recognized as  
80 negative regulators of the non-canonical NF- $\kappa$ B pathway. Hence, in all cell types  
81 cIAP1/2 associate in a heterocomplex with TNF receptor associated factor (TRAF)2,  
82 TRAF3 and NF- $\kappa$ B-inducing kinase (NIK), whereby they induce K-48 ubiquitination of  
83 NIK, resulting in its continuous proteasomal degradation (Zarnegar *et al*, 2008;  
84 Varfolomeev *et al*, 2007; Vince *et al*, 2007). Breakdown of the TRAF2-TRAF3-cIAP1/2-  
85 NIK complex either following ligation of TNF superfamily receptors that recruit TRAF2-  
86 TRAF3 in their intracellular domain (e.g. TNFR2, LT $\beta$ R, CD40) or by cIAP1/2 depletion,  
87 liberates NIK, which initiates the cascade necessary for nuclear translocation of the  
88 non-canonical NF- $\kappa$ B transcription factors RelB and p52 (Vallabhapurapu *et al*, 2008;  
89 Matsuzawa *et al*, 2008)

90 In the present study we demonstrate a necessary role for cIAP1/2 in sustaining  
91  $\gamma\delta$ T17 cells and ILC3 at the late neonatal and prepubescent stages of life, and thus  
92 impacting the magnitude of inflammatory and anti-bacterial immune responses.  
93 Deficiency in cIAP1/2 begun to have an impact only during late neonatal life by reducing  
94 expression of the lineage defining transcription factors cMAF and ROR $\gamma$ t, which was  
95 followed by an apparent block in cytokine-induced proliferation. When animals entered

96 prepubescence and early adolescence, cIAP1/2 deficiency resulted in progressive loss  
97 of  $\gamma\delta$ T17 cells. This was independent of TNFR1 induced canonical NF- $\kappa$ B or cell death. In  
98 contrast, cIAP1/2-deficient prepubescent  $\gamma\delta$ T17 cells displayed enhanced nuclear  
99 translocation of RelB, which demonstrates evidence of overt activation of the non-  
100 canonical NF- $\kappa$ B pathway. Intestinal ILC3 also relied on intact cIAP1/2 during the same  
101 time period, with their numbers being drastically reduced in adulthood. Paucity in ILC3  
102 coincided with ILF involution. Mice with targeted deletion of cIAP1/2 in  $\gamma\delta$ T17 cells and  
103 ILC3 responded sub-optimally to cutaneous inflammatory challenge and failed to control  
104 intestinal bacterial infection.

105

## 106 **Results**

107 **Paucity of  $\gamma\delta$ T17 cells in the absence of the E3 ubiquitin ligases cIAP1 and cIAP2**  
108 Using acute, SMAC mimetic (SM) driven antagonization and in vitro techniques, we  
109 showed before that cIAP1/2 are important for  $T_{H}17$  differentiation through modulation of  
110 the non-canonical NF- $\kappa$ B pathway (Rizk *et al*, 2019). In order to understand the *in vivo*  
111 importance of cIAP1 and cIAP2 in ROR $\gamma$ t-expressing immune cells, we crossed *Rorc-*  
112 *Cre* (ROR $\gamma$ t<sup>CRE</sup>) mice (Eberl & Litman, 2004) with mice that were floxed for *Birc2*  
113 (cIAP1<sup>F/F</sup>) and knocked out for *Birc3* (cIAP2<sup>-/-</sup>) (Gardam *et al*, 2011). This generated  
114 mice with ROR $\gamma$ t-driven deletion of cIAP1 (referred to thereafter as  $\Delta$ IAP1) and  
115 generalized deletion of cIAP2 (referred to thereafter as  $\Delta$ IAP2), as well as the  
116 corresponding Cre-negative littermate controls (wild-type; WT) (Fig 1A).  $\Delta$ IAP1 and  
117  $\Delta$ IAP1/2 mice were viable, produced offspring at expected rates, and did not develop  
118 any observable spontaneous disease phenotypes. They contained a full set of lymph  
119 nodes (inguinal, brachial, axillary and mesenteric) and Peyer's patches indicating

120 unperturbed lymphoid tissue development, while total numbers of CD4<sup>+</sup> T and B cells  
121 were normal but  $\gamma\delta$  T were slightly elevated (Fig S1A).

122 We next analyzed some of the major IL-17-producing populations in lymph node  
123 (LN) and small intestinal and colonic lamina propria (sILP; cLP). Compared to littermate  
124 controls,  $\Delta$ IAP1/2 mice produced slightly elevated levels of IL-17A within the  
125 CD4<sup>+</sup>TCR $\beta$ <sup>+</sup> compartment in the LN (pool of inguinal, brachial, axillary) but not the gut  
126 (Fig S1B), suggesting that in these animals, steady-state production of IL-17A by CD4<sup>+</sup>  
127 T cells is not defective. Staining for IL-22 following overnight stimulation with IL-23  
128 yielded the same answer (Fig S1C). However, there was a marked reduction in  $\gamma\delta$ -  
129 associated IL-17A and IL-22 production in LN (Fig 1B) and IL-17A in the gut (Fig 1C).  
130 This was accompanied by a dramatic loss in LN TCR $\gamma\delta$ <sup>+</sup>CD27<sup>-</sup>CD44<sup>hi</sup>CCR6<sup>+</sup>, which are  
131 the IL-17-producing  $\gamma\delta$  T cells (Ribot *et al*, 2009; Haas *et al*, 2009) (Fig 1D and Fig  
132 S1D), and gut Tbet<sup>+</sup>RORyt<sup>+</sup> (Kadekar *et al*, 2020) (Fig 1E)  $\gamma\delta$ T17 cell numbers.  
133 Although cIAP1 and cIAP2 individually did not contribute to this phenotype in the LN,  
134  $\Delta$ IAP2 mice had significantly reduced Tbet<sup>+</sup>RORyt<sup>+</sup>  $\gamma\delta$  T cell numbers in the gut (Fig  
135 1E). We additionally found significantly reduced  $\gamma\delta$ T17 cells in the lungs of  $\Delta$ IAP2 mice  
136 (Fig S1E). Similar to  $\gamma\delta$ T17 cells, there were significantly reduced non-CD4 IL-17-  
137 producing lymphocytes in the LNs of  $\Delta$ IAP1/2 mice (Fig S1F).

138 In the skin, CD3<sup>lo</sup>V $\gamma$ 5<sup>-</sup>TCR $\gamma\delta$ <sup>+</sup>CCR6<sup>+</sup> cells, which represent the  $\gamma\delta$ T17 population  
139 (Haas *et al*, 2009, 2012), were also reduced significantly in the absence of cIAP1 and  
140 cIAP2 (Fig 2A). When we analyzed the two major  $\gamma\delta$ T17 subpopulations (V $\gamma$ 4<sup>+</sup> versus  
141 V $\gamma$ 4<sup>-</sup>; V $\gamma$  nomenclature by Heilig and Tonegawa; (Heilig & Tonegawa, 1986)), we found  
142 that in the skin cIAP1 but not cIAP2 was required for V $\gamma$ 4<sup>-</sup> cells, whereas the V $\gamma$ 4-  
143 expressing population was only affected by the absence of both cIAP1 and cIAP2 (Fig

144 2B). In the LN, we did not observe differential regulation of either V $\gamma$ 4 $^{+}$  or V $\gamma$ 4 $^{-}$  cells (Fig  
145 S2A). Collectively, this data suggests that cIAP1/2 are important for the development  
146 and/or homeostatic maintenance of  $\gamma\delta$ T17 cells. Our findings additionally pinpoint a  
147 differential and non-redundant role of cIAP1 and cIAP2 in these cells that is organ and  
148 subset specific. In this regard, whereas skin  $\gamma\delta$ T17 cells depended more on cIAP1, gut  
149  $\gamma\delta$ T17 cells depended more on cIAP2.

150

### 151 **Cell-intrinsic requirement for cIAP1 and cIAP2 in $\gamma\delta$ T17 cells**

152 Next, we investigated whether the defect we observed in  $\Delta$ IAP1/2 mice was cell-  
153 intrinsic. To this end we set up mixed bone marrow (BM) chimeras where WT  
154 CD45.1 $^{+}$ CD45.2 $^{+}$  hosts were sub-lethally irradiated and reconstituted with a mixture of  
155 1:1 CD45.1 $^{+}$  WT and CD45.2 $^{+}$   $\Delta$ IAP1/2 BM cells (Fig 3A). We found that, under these  
156 conditions, WT LN  $\gamma\delta$ T17 cells outcompeted their  $\Delta$ IAP1/2 counterparts (Fig 3B),  
157 indicating the phenotype we observed in intact mice was cell intrinsic. Interestingly,  
158 CD27 $^{+}$   $\gamma\delta$  T cells derived from  $\Delta$ IAP1/2 BM were slightly less competitive than WT (Fig  
159 3B). In contrast, both CD3 $^{-}$  populations and B cells from  $\Delta$ IAP1/2 BM were more  
160 competitive than their WT counterparts (Fig 3C). This indicated that the reduced  
161 competitiveness of  $\gamma\delta$ T17 and CD27 $^{+}$   $\gamma\delta$  T cells was not due to defective  $\Delta$ IAP1/2 BM  
162 reconstitution. We could not reconstitute gut RORyt $^{+}$ Tbet $^{+}$   $\gamma\delta$ T17 cells irrespective of  
163 the BM source (Fig 3D), suggesting that this population requires either thymus-  
164 originated  $\gamma\delta$  T cells or a neonatal microenvironment to develop fully. In contrast, lack of  
165 cIAP1 and cIAP2 did not impinge on the reconstitution of gut Tbet $^{+}$ RORyt $^{-}$   $\gamma\delta$  T cells  
166 (Fig 3E). Likewise, we could only recover WT LN  $\gamma\delta$ T17 cells when we reconstituted  
167  $\Delta$ IAP1/2 hosts with WT or a 1:1 mix of WT and  $\Delta$ IAP1/2 BM (Fig S3A-B), while CD27 $^{+}$

168  $\gamma\delta$  T cells from WT or  $\Delta$ IAP1/2 BM cells were equally competitive (Fig S3B). As before,  
169 we could not reconstitute ROR $\gamma$ t<sup>+</sup>Tbet<sup>+</sup>  $\gamma\delta$ T17 cells in the gut (Fig S3C).

170 As  $\gamma\delta$ T17 cells develop perinatally in the thymus and undergo a rapid neonatal re-  
171 programming within the tissues they localize at, we reasoned that if generated from BM  
172 stem cells, they might have different developmental or homeostatic requirements for  
173 cIAP1 and cIAP2. To address this issue, we purified  $\gamma\delta$  T cells from the thymi of 1-day  
174 old WT or  $\Delta$ IAP1/2 mice and transferred them to RAG1<sup>-/-</sup> recipients (Fig 3F). We found  
175 that 12 weeks post transfer, the  $\gamma\delta$ T17 cell compartment was reconstituted in the LN,  
176 however, we recovered significantly more WT than  $\Delta$ IAP1/2 cells (Fig 3G). As with the  
177 BM chimeras, we could not reconstitute intestinal ROR $\gamma$ t<sup>+</sup>Tbet<sup>+</sup>  $\gamma\delta$ T17 cells, suggesting  
178 that this population requires a neonatal microenvironment (Fig S3D). Reconstitution of  
179 CD27<sup>+</sup>  $\gamma\delta$  T cells was independent of cIAP1 and cIAP2 (Fig 3G). Taken together our  
180 data show that  $\gamma\delta$ T17 cells require cIAP1 and cIAP2 intrinsically.

181

182 **The impact of cIAP1 and cIAP2 on  $\gamma\delta$ T17 cells is independent of TNF induced  
183 canonical NF- $\kappa$ B and cell death**

184 In addition to preventing spontaneous activation of the non-canonical NF- $\kappa$ B pathway,  
185 cIAP1/2 are necessary to convey the canonical NF- $\kappa$ B downstream of TNFR1 whereas  
186 in their absence, TNF-TNFR1 interactions can lead to RIPK1-mediated cell death via  
187 apoptosis or necroptosis (Annibaldi & Meier, 2018). Mice deficient in TNFR1 had an  
188 intact  $\gamma\delta$ T17 cell population (Fig S4A), suggesting that the canonical NF- $\kappa$ B pathway  
189 downstream of TNFR1 is not responsible for the phenotype of  $\Delta$ IAP1/2 mice. Since TNF  
190 is highly upregulated during the weaning reaction (Al Nabhani *et al*, 2019), we next  
191 investigated whether TNF induced cell death played a role. To achieve this, we initially

192 analyzed mice that were deficient in cIAP2 and expressed a ubiquitin-associated (UBA)  
193 domain mutant form of cIAP1 unable to K48 ubiquitylate and suppress RIPK1 (Annibaldi  
194 *et al*, 2018). Thus, these mice are more sensitive to TNF induced cell death (Annibaldi  
195 *et al*, 2018). In UBA-mutant mice,  $\gamma\delta$ T17 cells were not affected (Fig S4B), suggesting  
196 that these cells are not susceptible to death by homeostatic levels of TNF. In order to  
197 test this directly in  $\Delta$ IAP1/2 mice, we began injecting 1-week old neonates with  
198 neutralizing anti-TNF antibody and until animals were 12-week old (Fig S4C). We could  
199 not rescue the  $\gamma\delta$ T17 population in either gut or LNs (Fig S4D-E), indicating that TNF  
200 induced death is unlikely to play a major role in regulating these cells in the absence of  
201 cIAP1/2. Therefore, TNF-TNFR1 interactions are not responsible for the  $\Delta$ IAP1/2  
202 phenotype, suggesting that overt activation of the non-canonical NF- $\kappa$ B pathway could  
203 play a key role.

204

205 **cIAP1 and cIAP2 are required for  $\gamma\delta$ T17 cell cycle progression and expression of  
206 cMAF and ROR $\gamma$ t during aging**

207 In order to assess the impact of cIAP1/2 on embryonic  $\gamma\delta$ T17 cell development, we  
208 enumerated thymic cell numbers in newborn  $\Delta$ IAP1/2 mice and found them similar to  
209 littermate controls (Fig 4A), despite efficient deletion of *Birc2* (cIAP1) (Fig S5A).  
210 Production of IL-17A/F were unchanged at this stage (Fig S5B). This suggested that the  
211 major impact of cIAP1/2 occurs post-embryonically. We therefore tracked LN  $\gamma\delta$ T17  
212 cells, defined phenotypically as CD27 $^{-}$ CD44 $^{\text{hi}}$ , during neonatal, post-neonatal (average  
213 weaning time at 3 weeks) and adult life (mating age of 8 weeks). We did not find any  
214 differences in cell numbers until week 5 of age (Fig 4B). This suggested that cIAP1 and  
215 cIAP2 are only required to sustain  $\gamma\delta$ T17 numbers following weaning. After week 5,

216  $\Delta$ IAP1/2  $\gamma\delta$ T17 cells failed to expand and began to decline progressively during aging  
217 (Fig 4B). In order to confirm that the cells are missing from adult life and have not  
218 converted to a non- $\gamma\delta$ T17 population, we crossed  $\Delta$ IAP1/2 with the ROSA26-LSL-RFP  
219 strain, so that RFP permanently marks all current and “ex” RORyt-expressing cells. We  
220 found no evidence of  $\gamma\delta$ T17 conversion to other populations (Fig 4C). This data  
221 suggested that cIAP1/2 regulate a checkpoint in early adult life that manifests during  
222 aging.

223 We next investigated what this checkpoint was. The inability of the cells to increase  
224 in numbers during aging, raised the hypothesis that cIAP1/2 may be regulating  
225 responsiveness to cytokines that induce proliferation. We thus isolated 4-week old LN  
226 cells and treated them in vitro with IL-7 or a combination of IL-1 $\beta$ +IL-23. We found that  
227  $\Delta$ IAP1/2  $\gamma\delta$ T17 cells were slower in entering cell cycle with most cells stuck in G0 (Fig  
228 4D-E). This defect in proliferation was also observed following stimulation with either IL-  
229 2 or TCR cross-linking (Fig S5C). Therefore, cIAP1/2 are important for  $\gamma\delta$ T17 cell cycle  
230 progression.

231 We have shown before that ablation of cIAP1/2 in T cells downregulates cMAF, a  
232 lineage determining transcription factor for  $\gamma\delta$ T17 cells (Zuberbuehler *et al*, 2019), in a  
233 NIK- and RelB-dependent mechanism (Rizk *et al*, 2019). We thus hypothesized that  
234 lack of cIAP1/2 may influence expression of cMAF. In newborn thymus expression of  
235 cMAF as well as RORyt was unchanged (Fig S6A). At week 1 after birth we observed a  
236 slight reduction in the expression of RORyt and cMAF (Fig S6B). However, at week 3 of  
237 age, expression of RORyt and cMAF was significantly reduced (Fig 5A). Furthermore,  
238 we observed a modest but significant reduction in IL-17A production by 3-week old  
239  $\Delta$ IAP1/2  $\gamma\delta$ T17 cells (Fig 5B). In the intestine, RORyt $^+$   $\gamma\delta$  T cells express high levels of

240 CD127 (IL-7R $\alpha$ ) and intermediate levels of CD45 (Fig 5C). Due to lack of other reliable  
241 surface markers to identify these cells in the gut, we gated TCR $\gamma\delta^+$ CD45<sup>int</sup>CD127 $^+$  cells  
242 and quantified numbers as well as expression of RORyt and cMAF. Similar to the LNs,  
243 numbers in the siLP did not change in 4-week old  $\Delta$ IAP1/2 mice (Fig 5D), however there  
244 was a significant reduction in the levels of RORyt and cMAF (Fig 5E).

245 Furthermore, we investigated the expression of RelB in newborn thymic  $\gamma\delta$  T cells  
246 and found a significant upregulation of *Relb* mRNA in  $\Delta$ IAP1/2  $\gamma\delta$ T17 but not in CD27 $^+$   
247  $\gamma\delta$  T cells (Fig S6C). We additionally examined the extent of RelB nuclear translocation  
248 in  $\gamma\delta$ T17 cells from 4-week old WT,  $\Delta$ IAP2 and  $\Delta$ IAP1/2 mice. We found that the levels  
249 of nuclear RelB in  $\Delta$ IAP1/2  $\gamma\delta$ T17 cells were significantly higher by comparison to WT  
250 cells (Fig 5F), arguing for a role of the non-canonical NF- $\kappa$ B pathway in downregulation  
251 of RORyt and cMAF. Therefore, cIAP1/2 are required during late neonatal life in order to  
252 maintain expression of the transcription factors RORyt and cMAF and to sustain normal  
253  $\gamma\delta$ T17 numbers.

254

255 **Inflammation partially restores  $\gamma\delta$ T17 responses in the absence of cIAP1 and  
256 cIAP2**

257 Next, we investigated whether cytokines that activate  $\gamma\delta$ T17 cells could regulate  
258 expression of RORyt and cMAF from 4-week old mice. Culture with IL-7 did not  
259 influence expression of either transcription factors (Fig 6A-C), however, a combination  
260 of IL-1 $\beta$  and IL-23 resulted in partial restoration of RORyt but not cMAF in  $\Delta$ IAP1/2  
261  $\gamma\delta$ T17 cells (Fig 6A-C). Interestingly, IL-1 $\beta$ +IL-23 resulted in downregulation of cMAF in  
262 WT cells (Fig 6A-B). We additionally observed that the  $\Delta$ IAP1/2  $\gamma\delta$ T17 cells that  
263 acquired RORyt, were the cells that entered G1 in response to IL-1 $\beta$ +IL-23 and to a

264 lesser extent in response to IL-7 (Fig S7). In the imiquimod(IMQ)-driven psoriasisiform  
265 dermatitis model, IL-23, IL-1 $\beta$  and IL-7 drive  $\gamma\delta$ T17 cell expansion as well as production  
266 of IL-17 and IL-22 in the LN and skin (Michel *et al*, 2012; Cai *et al*, 2011, 2014). We thus  
267 treated WT,  $\Delta$ IAP1,  $\Delta$ IAP2, and  $\Delta$ IAP1/2 4-week old mice with IMQ for seven days and  
268 assessed expression of RORyt and cMAF in  $\gamma\delta$ T17 cells. We found that IMQ treatment  
269 partially restored expression of both RORyt and cMAF in  $\Delta$ IAP1/2  $\gamma\delta$ T17 cells in the  
270 LNs (Fig 6D), suggesting that inflammation can rescue the  $\Delta$ IAP1/2 phenotype.

271 We then investigated whether rescue of RORyt and cMAF was sufficient for  
272  $\Delta$ IAP1/2  $\gamma\delta$ T17 cells to mount an immune response. We observed that despite an  
273 increase in Ki67 expression (Fig S8A),  $\Delta$ IAP1/2  $\gamma\delta$ T17 numbers did not increase in  
274 either the LNs or skin (Fig 6E). Evaluation of cytokine production revealed substantial  
275 regional differences between LN and skin in  $\Delta$ IAP1/2 mice. Thus, whereas in the LN,  
276  $\Delta$ IAP1/2  $\gamma\delta$ T17 cells increased (albeit significantly less than their WT,  $\Delta$ IAP1 and  $\Delta$ IAP2  
277 counterparts) their production of IL-17A following IMQ treatment, this was not the case  
278 in the skin (Fig 6F). In contrast, IL-22 production in LNs was significantly reduced while  
279 it was relatively normal in the skin (Fig 6G). The CD4 $^+$  T cell response to IMQ was not  
280 defective and slightly stronger in  $\Delta$ IAP1/2 mice (Fig S8B). The extent of skin  
281 inflammation, as measured by epidermal thickening, was not different between  $\Delta$ IAP1/2  
282 and control mice, reflecting both the partial rescue of the  $\gamma\delta$ T17 as well as the slightly  
283 exaggerated CD4 $^+$  T cell response (Fig S8C).

284 The data suggest that although at a young age cIAP1/2 regulate proliferation,  
285 transcriptional stability and cytokine production, strong inflammatory stimuli can, to a  
286 certain extent, overcome this regulatory checkpoint and revive  $\gamma\delta$ T17 cell responses.  
287 These results additionally indicate that the extrathymic expression and biological impact

288 thereafter of ROR $\gamma$ t and cMAF can be dynamic and under the control of multiple  
289 microenvironment cues.

290

291 **clAP1 and clAP2 are required for intestinal ILC3 during aging and for sustaining  
292 ILF integrity**

293 ILC3 share many functional characteristics and transcription factor requirements with  
294  $\gamma\delta$ T17 cells, including constitutive expression of ROR $\gamma$ t and cMAF (Zuberbuehler *et al*,  
295 2019; Parker *et al*, 2019). We therefore investigated the impact of clAP1 and clAP2  
296 deficiency in intestinal ILC3 populations. Similar to  $\gamma\delta$ T17 cells, LP Tbet $^+$  and Tbet $^-$  ILC3  
297 numbers were reduced in  $\Delta$ clAP1/2 mice (Fig 7A-C and Fig S9A). As expected ILC2  
298 numbers were not affected (Fig S9B). Next, we tested whether  $\Delta$ clAP1/2 ILC3 converted  
299 to an ROR $\gamma$ t $^-$  population and hence performed a lineage tracing experiment using the  
300 ROR $\gamma$ t-RFP reporter mice described above. We found that within the ILC population,  
301 there was a 10-fold reduction in RFP $^+$  cell numbers, suggesting that in the absence of  
302 clAP1 and clAP2, there is loss of ILC3 rather than conversion to a non-ILC3 population  
303 (Fig S9C). Similar to  $\gamma\delta$ T17 cells, we found that ILC3 numbers did not expand post  
304 weaning (Fig 7D). Next, we investigated whether the ILC3 defect in  $\Delta$ clAP1/2 mice was  
305 cell-intrinsic. To this end, using mixed BM chimeras, we found that WT ILC3  
306 outcompeted their  $\Delta$ clAP1/2 counterparts (Fig 7E-F), indicating that the phenotype we  
307 observed in intact mice was cell-intrinsic. There was equal reconstitution capacity of  
308 GATA3-expressing ILC2 derived from WT or  $\Delta$ clAP1/2 BM (Fig S9D), demonstrating the  
309 specificity of the defect within ROR $\gamma$ t-expressing populations. We obtained similar  
310 results when we reconstituted  $\Delta$ clAP1/2 hosts with a 1:1 mix of WT and  $\Delta$ clAP1/2 BM (Fig

311 7G and Fig S9E). Further, cIAP1 and 2 deficient ILC3 cells were not rescued by  
312 treatment with anti-TNF (Fig S9F).

313 ILC3 are necessary for the maturation of cryptopatches to ILFs during the first  
314 weeks of life.  $\Delta$ IAP1/2 mice had severely defective ILFs (Fig 7H). ILFs in these mice  
315 were either absent or reduced in size (Fig 7H). Despite the lack of ILFs, production of  
316 IgA was not defective (Fig S9G). Collectively, this data shows that cIAP1 and cIAP2 are  
317 necessary for intestinal ILC3 to expand during the post-weaning period, and to induce  
318 formation of ILFs.

319

320 **cIAP1 and cIAP2 are necessary to protect against *Citrobacter rodentium* infection**

321 It has been demonstrated that ILC3 are important to control infection by the attaching  
322 and effacing bacterium *Citrobacter rodentium* (Bauché *et al*, 2020; Guo *et al*, 2015,  
323 2014), a widely used model for human enteropathogenic *E. coli* infections (Silberger *et*  
324 *al*, 2017) .We therefore reasoned that  $\Delta$ IAP1/2 mice may be defective in mounting a  
325 protective response to *C. rodentium*. We infected  $\Delta$ IAP1/2 mice and their respective  
326 controls with  $2 \times 10^9$  CFU of *C. rodentium* through oral gavage and followed weight loss  
327 as a surrogate marker for disease. We found that by 11 days after infection  $\Delta$ IAP1/2  
328 mice lost approximately 20% of their body weight, while all other strains did not (Fig 8A).  
329 At this time point and due to ethical constraints, all animals were sacrificed and we  
330 analyzed bacterial loads and the immune response in the colon.  $\Delta$ IAP1/2 mice had  
331 significantly higher colonic bacterial load than controls (Fig 8B). This was associated  
332 with compromised IL-22 production from the ILC3 compartment (Fig 8C-D).

333 Although ILC3 are important to protect from *C. rodentium* infection, a  $T_{H}17$  and  
334  $T_{H}22$  response is also required, as evidenced by susceptibility of  $RAG1^{-/-}$  mice to this

335 pathogen (Silberger *et al*, 2017). We therefore additionally analyzed the CD4<sup>+</sup> T cell  
336 response in the colon. Numbers of total CD4<sup>+</sup> T cells were not changed in infected  
337 ΔIAP1/2 mice (Fig 8E). However, there was a significant reduction in RORyt<sup>+</sup>Tbet<sup>-</sup> CD4<sup>+</sup>  
338 T cells (Fig 8E), which was accompanied by reduced levels of IL-17A (Fig 8F). Despite  
339 normal numbers of RORyt<sup>+</sup>Tbet<sup>+</sup> CD4<sup>+</sup> T cells (Fig 8E), IL-17A<sup>+</sup>IFN- $\gamma$ <sup>+</sup> cells were  
340 significantly reduced in infected ΔIAP1/2 mice (Fig 8F). However, production of IL-22  
341 was not defective in the absence of cIAP1 and cIAP2 (Fig 8F). Collectively, our data  
342 suggest that cIAP1 and cIAP2 are required within the ILC3 and T<sub>H</sub>17 compartments to  
343 control intestinal bacterial infection.

344

## 345 **Discussion**

346 In the present study we demonstrate that the E3 ubiquitin ligases cIAP1 and cIAP2 are  
347 necessary for  $\gamma\delta$ T17 cells to transition through to prepubescent life by regulating  
348 cytokine-mediated proliferation and stable expression of the lineage defining  
349 transcription factors cMAF and RORyt. Thus, during aging, cIAP1 and cIAP2 are  
350 required in a cell-intrinsic manner to maintain cMAF and RORyt levels and to allow cells  
351 to enter cell cycle in response to IL-7, IL-1 $\beta$  and IL-23. Consequently,  $\gamma\delta$ T17-driven  
352 inflammatory responses in the skin and draining LNs of prepubescent ΔIAP1/2 mice are  
353 blunted despite normal cell numbers, while by the time animals reach adulthood,  $\gamma\delta$ T17  
354 populations are deficient in gut, skin and LNs. Mechanistically, our data suggest that  
355 this is independent of TNF and TNFR1 and most likely through overt activation of the  
356 non-canonical NF- $\kappa$ B pathway. Similar to  $\gamma\delta$ T17, ILC3 required cIAP1 and cIAP2  
357 expression during the post-weaning period in order to expand, be maintained until adult  
358 life, and induce formation of intestinal ILFs. The ILC3 deficit in ΔIAP1/2 mice together

359 with a defective T<sub>H</sub>17 response, correlated with a profound inability to control intestinal  
360 bacterial infection.

361 The IL-17-producing  $\gamma\delta$  T cell subset is an innate-like unconventional lymphocyte  
362 that is important in many immunological processes ranging from anti-microbial  
363 protection to pathogenic inflammation and cancer (Patil *et al*, 2015).  $\gamma\delta$ T17 cells are  
364 pre-programmed and functionally mature in the embryonic thymus in mouse and human  
365 (Ribot *et al*, 2009; Haas *et al*, 2012). They are exported into peripheral and secondary  
366 lymphoid tissues after birth, and evidence suggests that they go through a second wave  
367 of transcriptional and functional programming during neonatal life within the tissues they  
368 occupy (Kadekar *et al*, 2020; Wiede *et al*, 2017). The molecular cues that  $\gamma\delta$ T17 cells  
369 receive within the tissues during that period are obscure. Our data show that the E3  
370 ligases cIAP1 and cIAP2 are required during late neonatal and early prepubescent life  
371 in a cell-intrinsic manner for cytokine-induced proliferation, to sustain transcriptional  
372 stability and allow optimal inflammatory responses. This work establishes cIAP1/2 as  
373 critical molecular regulators of committed tissue-resident  $\gamma\delta$ T17 cells, and underpins the  
374 existence and importance of post-thymic temporal events necessary for these cells to  
375 be maintained during aging.

376 cIAP1/2 are central for TNFR1 induced canonical NF- $\kappa$ B activation and cell death  
377 (Mahoney *et al*, 2008) , and necessary to suppress overt non-canonical NF- $\kappa$ B signaling  
378 (Vallabhapurapu *et al*, 2008; Zarnegar *et al*, 2008) . TNFR1 induced apoptosis and  
379 necroptosis are fundamental biological processes regulating cell growth during  
380 development, homeostatic turnover and even inflammatory diseases (Kalliolias &  
381 Ivashkiv, 2016). The two NF- $\kappa$ B pathways on the other hand are synonymous with cell  
382 survival, proliferation and differentiation in ubiquitous cell populations (Hayden & Ghosh,

383 2011). In T cells they are mostly active downstream of TNF superfamily receptors and  
384 the TCR (Oh & Ghosh, 2013). Although the role of several TNF superfamily receptors  
385 and ligands have been studied in  $\gamma\delta$  T cells (Powolny-Budnicka *et al*, 2011; Shibata *et*  
386 *al*, 2011; Silva-Santos *et al*, 2005), the importance of the signaling components of the  
387 NF- $\kappa$ B pathway had not been thoroughly investigated. Genetic and pharmacological  
388 perturbations of the TNFR1 signaling, combined with aberrant nuclear translocation of  
389 RelB that it is the cIAP1/2-mediated control of non-canonical NF- $\kappa$ B that is required for  
390 the maintenance of  $\gamma\delta$ T17 cells. This agrees with CD27, a TNF superfamily receptor  
391 and potent activator of non-canonical NF- $\kappa$ B (Ramakrishnan *et al*, 2004), suppressing  
392 the  $\gamma\delta$ T17 differentiation program (Ribot *et al*, 2009). Importantly, deletion of NIK, the  
393 kinase targeted by cIAP1/2 and responsible for activating the non-canonical NF- $\kappa$ B  
394 cascade, did not affect  $\gamma\delta$ T17 cell development or homeostasis (Mair *et al*, 2015). This  
395 strongly suggests that it is the “brake” imposed by cIAP1/2 in order to avoid over  
396 activation of non-canonical NF- $\kappa$ B that is critical and not its baseline activity.

397 There are a number of transcription factors that are important for the development  
398 of  $\gamma\delta$ T17 cells (Parker & Ciofani, 2020) . Ciofani and co-workers showed that cMAF acts  
399 early in embryogenesis to allow robust expression of ROR $\gamma$ t and thus promote  
400 specification and stability of the  $\gamma\delta$ T17 lineage (Zuberbuehler *et al*, 2019). How cMAF  
401 and ROR $\gamma$ t expression is regulated, however, in  $\gamma\delta$ T17 cells is not well-defined. Herein,  
402 we demonstrate that loss of cIAP1/2 results in the progressive downmodulation of cMAF  
403 and ROR $\gamma$ t after birth, providing a molecular understanding of how lineage defining  
404 transcription factors are regulated in these cells. Although loss of cMAF and ROR $\gamma$ t  
405 during embryonic development resulted in rapid loss of  $\gamma\delta$ T17 cells or their progenitors  
406 in the thymus (Zuberbuehler *et al*, 2019; Shibata *et al*, 2011) , we observed that in

407  $\Delta$ IAP1/2 mice, cells persist for at least 2 weeks without either transcription factor. Thus,  
408 it appears that during neonatal life the impact of cMAF and RORyt in  $\gamma\delta$ T17 cells is less  
409 pronounced. The exact molecular steps leading to cIAP1/2-dependent regulation of  
410 cMAF and RORyt are currently unclear. Our previous work showed that following  
411 cIAP1/2 inhibition, NIK-mediated RelB nuclear translocation suppressed expression of  
412 cMAF in  $T_H$ 17 cells (Rizk *et al*, 2019). It is plausible therefore, that accumulation of non-  
413 canonical NF- $\kappa$ B signaling directly suppresses cMAF, which subsequently suppresses  
414 RORyt. Intriguingly, cytokine stimulation and inflammation could partially restore  
415 expression of cMAF and RORyt, indicating a certain degree of transcriptional plasticity.

416 In addition to  $\gamma\delta$ T17 cells, cIAP1/2 were necessary for the establishment of a  
417 normal ILC3 population during the post-weaning period in the gut and the formation of  
418 ILFs, as well as protection from intestinal extracellular bacterial infection. During  
419 infection, we additionally found that cIAP1/2, were critical for the generation of IL-17<sup>+</sup>  
420 and IL-17<sup>+</sup>IFN- $\gamma$ <sup>+</sup> CD4+ T cells, which have been associated with protection against  
421 pathogens, or tissue damage in the context of inflammation (Omenetti *et al*, 2019). We  
422 and others have previously reported that the cIAP-non-canonical NF- $\kappa$ B axis is  
423 necessary for  $T_H$ 17 differentiation and successful IL-17-driven responses (Rizk *et al*,  
424 2019; Kawalkowska *et al*, 2019), while NIK was shown to be important for the  
425 generation of neuropathogenic  $T_H$ 17 cells (Lacher *et al*, 2018). Moreover, NIK  
426 expression and activation of the non-canonical NF- $\kappa$ B pathway in dendritic cells  
427 indirectly regulates maintenance of both  $T_H$ 17 cells and ILC3 (Jie *et al*, 2018). Our  
428 current data, extend and broaden the immunological importance of this pathway. We  
429 would like to propose that through regulation of non-canonical NF- $\kappa$ B, cIAP1/2 are  
430 master regulators of innate and adaptive type-3 immunity. Their requirement is

431 necessary during neonatal life to establish functional innate and innate-like type-3  
432 immune cell populations, whereas in the adult they support differentiation of antigen-  
433 dependent adaptive type-3 cells.

434

435 **References**

436 Annibaldi A & Meier P (2018) Checkpoints in TNF-Induced Cell Death: Implications in  
437 Inflammation and Cancer. *Trends Mol Med* 24: 49–65

438 Annibaldi A, Wicky John S, Vanden Berghe T, Swatek KN, Ruan J, Liccardi G, Bianchi  
439 K, Elliott PR, Choi SM, Van Coillie S, *et al* (2018) Ubiquitin-Mediated Regulation of  
440 RIPK1 Kinase Activity Independent of IKK and MK2. *Mol Cell* 69: 566-580.e5

441 Bauché D, Joyce-Shaikh B, Fong J, Villarino A V, Ku KS, Jain R, Lee Y-C, Annamalai L,  
442 Yearley JH & Cua DJ (2020) IL-23 and IL-2 activation of STAT5 is required for  
443 optimal IL-22 production in ILC3s during colitis

444 Bouladoux N, Harrison OJ & Belkaid Y (2017) The Mouse Model of Infection with  
445 *Citrobacter rodentium*. *Curr Protoc Immunol* 119: 19.15.1-19.15.25

446 Cahenzli J, Köller Y, Wyss M, Geuking MB & McCoy KD (2013) Intestinal Microbial  
447 Diversity during Early-Life Colonization Shapes Long-Term IgE Levels. *Cell Host*  
448 *Microbe* 14: 559–570

449 Cai Y, Shen X, Ding C, Qi C, Li K, Li X, Jala VR, Zhang H ge, Wang T, Zheng J, *et al*  
450 (2011) Pivotal Role of Dermal IL-17-Producing gd T Cells in Skin Inflammation.  
451 *Immunity* 35: 596–610

452 Cai Y, Xue F, Fleming C, Yang J, Ding C, Ma Y, Liu M, Zhang HG, Zheng J, Xiong N, *et*  
453 *al* (2014) Differential developmental requirement and peripheral regulation for  
454 dermal V $\gamma$ 34 and V $\gamma$ 36T17 cells in health and inflammation. *Nat Commun* 5: 1–14

455 Chen YS, Chen IB, Pham G, Shao TY, Bangar H, Way SS & Haslam DB (2020) IL-17-  
456 producing  $\gamma\delta$  T cells protect against *Clostridium difficile* infection. *J Clin Invest* 130:  
457 2377–2390

458 Conti HR, Peterson AC, Brane L, Huppler AR, Hernández-Santos N, Whibley N, Garg  
459 A V., Simpson-Abelson MR, Gibson GA, Mamo AJ, et al (2014) Oral-resident  
460 natural Th17 cells and  $\gamma\delta$  T cells control opportunistic *Candida albicans* infections.  
461 *J Exp Med* 211: 2075–2084

462 Eberl G (2016) Immunity by equilibrium. *Nat Rev Immunol* 16: 524–532

463 Eberl G & Litman DR (2004) Thymic origin of intestinal  $\alpha\beta$  T cells revealed by fate  
464 mapping of ROR $\gamma$ t<sup>+</sup> cells. *Science* (80- ) 305: 248–251

465 Fleming C, Cai Y, Sun X, Jala VR, Xue F, Morrissey S, Wei YL, Chien YH, Zhang HG,  
466 Haribabu B, et al (2017) Microbiota-activated CD103<sup>+</sup> DCs stemming from  
467 microbiota adaptation specifically drive  $\gamma\delta$ T17 proliferation and activation.  
468 *Microbiome* 5: 1–15

469 Gardam S, Turner VM, Anderton H, Limaye S, Basten A, Koentgen F, Vaux DL, Silke J  
470 & Brink R (2011) Deletion of cIAP1 and cIAP2 in murine B lymphocytes  
471 constitutively activates cell survival pathways and inactivates the germinal center  
472 response. *Blood* 117: 4041–4051

473 Guo X, Liang Y, Zhang Y, Lasorella A, Kee BL & Fu YX (2015) Innate Lymphoid Cells  
474 Control Early Colonization Resistance against Intestinal Pathogens through ID2-  
475 Dependent Regulation of the Microbiota. *Immunity* 42: 731–743

476 Guo X, Qiu J, Tu T, Yang X, Deng L, Anders RA, Zhou L & Fu YX (2014) Induction of  
477 innate lymphoid cell-derived interleukin-22 by the transcription factor STAT3  
478 mediates protection against intestinal infection. *Immunity*

479 Gury-BenAri M, Thaiss CA, Serafini N, Winter DR, Giladi A, Lara-Astiaso D, Levy M,  
480 Salame TM, Weiner A, David E, *et al* (2016) The Spectrum and Regulatory  
481 Landscape of Intestinal Innate Lymphoid Cells Are Shaped by the Microbiome. *Cell*  
482 166: 1231-1246.e13

483 Haas JD, Malinarich González FH, Schmitz S, Chennupati V, Föhse L, Kremmer E,  
484 Förster R & Prinz I (2009) CCR6 and NK1.1 distinguish between IL-17A and IFN- $\gamma$ -  
485 producing  $\gamma\delta$  effector T cells. *Eur J Immunol* 39: 3488–3497

486 Haas JD, Ravens S, Düber S, Sandrock I, Oberdörfer L, Kashani E, Chennupati V,  
487 Föhse L, Naumann R, Weiss S, *et al* (2012) Development of Interleukin-17-  
488 Producing  $\gamma\delta$  T Cells Is Restricted to a Functional Embryonic Wave. *Immunity* 37:  
489 48–59

490 Hayden MS & Ghosh S (2011) NF- $\kappa$ B in immunobiology. *Cell Res* 21: 223–244

491 Heilig JS & Tonegawa S (1986) Diversity of murine gamma genes and expression in  
492 fetal and adult T lymphocytes. *Nature* 322: 836–840

493 Hoytema van Konijnenburg DP, Reis BS, Pedicord VA, Farache J, Victora GD & Mucida  
494 D (2017) Intestinal Epithelial and Intraepithelial T Cell Crosstalk Mediates a  
495 Dynamic Response to Infection. *Cell* 171: 783-794.e13

496 Jie Z, Yang JY, Gu M, Wang H, Xie X, Li Y, Liu T, Zhu L, Shi J, Zhang L, *et al* (2018)  
497 NIK signaling axis regulates dendritic cell function in intestinal immunity and  
498 homeostasis. *Nat Immunol* 19: 1224–1235

499 Kadekar D, Agerholm R, Rizk J, Neubauer HA, Suske T, Maurer B, Viñals MT, Comelli  
500 EM, Taibi A, Moriggl R, *et al* (2020) The neonatal microenvironment programs  
501 innate  $\gamma\delta$  T cells through the transcription factor STAT5. *J Clin Invest* 130: 2496–  
502 2508

503 Kalliolias GD & Ivashkiv LB (2016) TNF biology, pathogenic mechanisms and emerging  
504 therapeutic strategies. *Nat Rev Rheumatol* 12: 49–62

505 Kawalkowska JZ, Ogbechi J, Venables PJ & Williams RO (2019) CIAP1/2 inhibition  
506 synergizes with TNF inhibition in autoimmunity by down-regulating IL-17A and  
507 inducing Tregs. *Sci Adv* 5: eaaw5422

508 Kiss EA, Vonarbourg C, Kopfmann S, Hobeika E, Finke D, Esser C & Diefenbach A  
509 (2011) Natural aryl hydrocarbon receptor ligands control organogenesis of intestinal  
510 lymphoid follicles. *Science* (80- ) 334: 1561–1565

511 Klose CSN, Kiss EA, Schwierzeck V, Ebert K, Hoyler T, D'Hargues Y, Göppert N,  
512 Croxford AL, Waisman A, Tanriver Y, *et al* (2013) A T-bet gradient controls the fate  
513 and function of CCR6-ROR $\gamma$ t + innate lymphoid cells. *Nature* 494: 261–265

514 Kruglov AA, Grivennikov SI, Kuprash D V., Winsauer C, Prepens S, Seleznik GM, Eberl  
515 G, Littman DR, Heikenwalder M, Tumanov A V., *et al* (2013) Nonredundant function  
516 of soluble Ita3 produced by innate lymphoid cells in intestinal homeostasis. *Science*  
517 (80- ) 342: 1243–1246

518 Lacher SM, Thurm C, Distler U, Mohebiany AN, Israel N, Kitic M, Ebering A, Tang Y,  
519 Klein M, Wabnitz GH, *et al* (2018) NF- $\kappa$ B inducing kinase (NIK) is an essential post-  
520 transcriptional regulator of T-cell activation affecting F-actin dynamics and TCR  
521 signaling. *J Autoimmun* 94: 110–121

522 St. Leger AJ, Desai J V., Drummond RA, Kugadas A, Almaghrabi F, Silver P,  
523 Raychaudhuri K, Gadjeva M, Iwakura Y, Lionakis MS, *et al* (2017) An Ocular  
524 Commensal Protects against Corneal Infection by Driving an Interleukin-17  
525 Response from Mucosal  $\gamma\delta$  T Cells. *Immunity* 47: 148-158.e5

526 Mahoney DJ, Cheung HH, Mrad RL, Plenchette S, Simard C, Enwere E, Arora V, Mak

527 TW, Lacasse EC, Waring J, *et al* (2008) Both cIAP1 and cIAP2 regulate TNF -  
528 mediated NF- B activation. *Proc Natl Acad Sci* 105: 11778–11783

529 Mair F, Joller S, Hoeppli R, Onder L, Hahn M, Ludewig B, Waisman A & Becher B  
530 (2015) The NF $\kappa$ B-inducing kinase is essential for the developmental programming  
531 of skin- resident and IL-17-producing  $\Gamma\delta$  T $\delta$  cells. *Elife* 4

532 Di Marco Barros R, Roberts NA, Dart RJ, Vantourout P, Jandke A, Nussbaumer O,  
533 Deban L, Cipolat S, Hart R, Iannitto ML, *et al* (2016) Epithelia Use Butyrophilin-like  
534 Molecules to Shape Organ-Specific  $\gamma\delta$  T Cell Compartments. *Cell* 167: 203-  
535 218.e17

536 Matsuzawa A, Tseng PH, Vallabhapurapu S, Luo JL, Zhang W, Wang H, Vignali DAA,  
537 Gallagher E & Karin M (2008) Essential cytoplasmic translocation of a cytokine  
538 receptor-assembled signaling complex. *Science* (80- ) 321: 663–668

539 McGinley AM, Sutton CE, Edwards SC, Leane CM, DeCourcey J, Teijeiro A, Hamilton  
540 JA, Boon L, Djouder N & Mills KHG (2020) Interleukin-17A Serves a Priming Role  
541 in Autoimmunity by Recruiting IL-1 $\beta$ -Producing Myeloid Cells that Promote  
542 Pathogenic T Cells. *Immunity* 52: 342-356.e6

543 Michel M-L, Pang DJ, Haque SFY, Potocnik AJ, Pennington DJ & Hayday AC (2012)  
544 Interleukin 7 (IL-7) selectively promotes mouse and human IL-17-producing cells.  
545 *Proc Natl Acad Sci* 109: 17549–17554

546 Al Nabhani Z, Dulauroy S, Marques R, Cousu C, Al Bounny S, Déjardin F, Sparwasser  
547 T, Bérard M, Cerf-Bensussan N & Eberl G (2019) A Weaning Reaction to  
548 Microbiota Is Required for Resistance to Immunopathologies in the Adult Cell Press

549 Oh H & Ghosh S (2013) NF- $\kappa$ B: Roles and regulation in different CD4+ T-cell subsets.  
550 *Immunol Rev* 252: 41–51

551 Omenetti S, Bussi C, Metidji A, Iseppon A, Lee S, Tolaini M, Li Y, Kelly G, Chakravarty  
552 P, Shoae S, *et al* (2019) The Intestine Harbors Functionally Distinct Homeostatic  
553 Tissue-Resident and Inflammatory Th17 Cells. *Immunity* 51: 77-89.e6

554 Parker ME, Barrera A, Wheaton JD, Zuberbuehler MK, Allan DSJ, Carlyle JR, Reddy  
555 TE & Ciofani M (2019) c-Maf regulates the plasticity of group 3 innate lymphoid  
556 cells by restraining the type 1 program. *J Exp Med*: jem.20191030

557 Parker ME & Ciofani M (2020) Regulation of  $\gamma\delta$  T Cell Effector Diversification in the  
558 Thymus. *Front Immunol* 11: 42

559 Patil RS, Bhat SA, Dar AA & Chiplunkar S V (2015) The Jekyll and Hyde story of IL17-  
560 Producing  $\gamma\delta$ T Cells. *Front Immunol* 6: 37

561 Powolny-Budnicka I, Riemann M, Tänzer S, Schmid RM, Hehlgans T & Weih F (2011)  
562 RelA and RelB transcription factors in distinct thymocyte populations control  
563 lymphotoxin-dependent interleukin-17 production in  $\gamma\delta$  T cells. *Immunity* 34: 364–  
564 374

565 Ramakrishnan P, Wang W & Wallach D (2004) Receptor-specific signaling for both the  
566 alternative and the canonical NF- $\kappa$ B activation pathways by NF- $\kappa$ B-inducing kinase.  
567 *Immunity* 21: 477–489

568 Ribot JC, DeBarros A, Pang DJ, Neves JF, Peperzak V, Roberts SJ, Girardi M, Borst J,  
569 Hayday AC, Pennington DJ, *et al* (2009) CD27 is a thymic determinant of the  
570 balance between interferon- $\gamma$ - and interleukin 17-producing  $\gamma\delta$  T cell subsets. *Nat  
571 Immunol* 10: 427–436

572 Rizk J, Kaplinsky J, Agerholm R, Kadekar D, Ivars F, Agace WW, Wei-Lynn Wong W,  
573 Szucs MJ, Myers SA, Carr SA, *et al* (2019) SMAC mimetics promote NIK-  
574 dependent inhibition of CD4+ TH17 cell differentiation. *Sci Signal* 12

575 Sandrock I, Reinhardt A, Ravens S, Binz C, Wilharm A, Martins J, Oberdörfer L, Tan L,

576 Lienenklaus S, Zhang B, *et al* (2018) Genetic models reveal origin, persistence and

577 non-redundant functions of IL-17-producing  $\gamma\delta$  T cells. *J Exp Med* 215: 3006–3018

578 Schindelin J, Arganda-Carreras I, Frise E, Kaynig V, Longair M, Pietzsch T, Preibisch S,

579 Rueden C, Saalfeld S, Schmid B, *et al* (2012) Fiji: an open-source platform for

580 biological-image analysis. *Nat Methods* 9: 676–682

581 Sheridan BS, Romagnoli PA, Pham QM, Fu HH, Alonzo F, Schubert WD, Freitag NE &

582 Lefrançois L (2013)  $\gamma\delta$  T Cells Exhibit Multifunctional and Protective Memory in

583 Intestinal Tissues. *Immunity* 39: 184–195

584 Shibata K, Yamada H, Sato T, Dejima T, Nakamura M, Ikawa T, Hara H, Yamasaki S,

585 Kageyama R, Iwakura Y, *et al* (2011) Notch-Hes1 pathway is required for the

586 development of IL-17-producing  $\gamma\delta$  T cells. *Blood* 118: 586–593

587 Silberger DJ, Zindl CL & Weaver CT (2017) *Citrobacter rodentium*: a model

588 enteropathogen for understanding the interplay of innate and adaptive components

589 of type 3 immunity. *Mucosal Immunol* 10: 1108–1117

590 Silke J & Meier P (2013) Inhibitor of apoptosis(IAP)proteins-modulators of cell death

591 and inflammation. *Cold Spring Harb Perspect Biol* 5: a008730

592 Silva-Santos B, Pennington DJ & Hayday AC (2005) Lymphotoxin-mediated regulation

593 of  $\gamma\delta$  cell differentiation by  $\alpha\beta$  T cell progenitors. *Science* (80- ) 307: 925–928

594 Spits H, Artis D, Colonna M, Diefenbach A, Di Santo JP, Eberl G, Koyasu S, Locksley

595 RM, McKenzie ANJ, Mebius RE, *et al* (2013) Innate lymphoid cells-a proposal for

596 uniform nomenclature. *Nat Rev Immunol* 13: 145–149

597 Steer CA, Mathä L, Shim H & Takei F (2020) Lung group 2 innate lymphoid cells are

598 trained by endogenous IL-33 in the neonatal period. *JCI Insight* 5

599 Vallabhapurapu S, Matsuzawa A, Zhang W, Tseng P-H, Keats JJ, Wang H, Vignali  
600 DAA, Bergsagel PL & Karin M (2008) Nonredundant and complementary functions  
601 of TRAF2 and TRAF3 in a ubiquitination cascade that activates NIK-dependent  
602 alternative NF- $\kappa$ B signaling. *Nat Immunol* 9: 1364–1370

603 Varfolomeev E, Blankenship JW, Wayson SM, Fedorova A V, Kayagaki N, Garg P,  
604 Zobel K, Dynek JN, Elliott LO, Wallweber HJA, et al (2007) IAP Antagonists Induce  
605 Autoubiquitination of c-IAPs, NF- $\kappa$ B Activation, and TNF $\alpha$ -Dependent Apoptosis.  
606 *Cell* 131: 669–681

607 Vince JE, Wong WWL, Khan N, Feltham R, Chau D, Ahmed AU, Benetatos CA,  
608 Chunduru SK, Condon SM, McKinlay M, et al (2007) IAP Antagonists Target cIAP1  
609 to Induce TNF $\alpha$ -Dependent Apoptosis. *Cell* 131: 682–693

610 Wiede F, Dudakov JA, Lu KH, Dodd GT, Butt T, Godfrey DI, Strasser A, Boyd RL &  
611 Tiganis T (2017) PTPN2 regulates T cell lineage commitment and  $\alpha\beta$  versus  $\gamma\delta$   
612 specification. *J Exp Med* 214: 2733–2758

613 Zarnegar BJ, Wang Y, Mahoney DJ, Dempsey PW, Cheung HH, He J, Shiba T, Yang X,  
614 Yeh WC, Mak TW, et al (2008) Noncanonical NF- $\kappa$ B activation requires coordinated  
615 assembly of a regulatory complex of the adaptors cIAP1, cIAP2, TRAF2 and  
616 TRAF3 and the kinase NIK. *Nat Immunol* 9: 1371–1378

617 Zuberbuehler MK, Parker ME, Wheaton JD, Espinosa JR, Salzler HR, Park E & Ciofani  
618 M (2019) The transcription factor c-Maf is essential for the commitment of IL-17-  
619 producing  $\gamma\delta$  T cells. *Nat Immunol* 20: 73–85

620

621

622 **Materials and methods**

623 **Mice**

624 All animals were bred and maintained in-house at DTU health tech with the approval of  
625 the Danish animal experiments inspectorate. clAP1<sup>ff</sup> and clAP1<sup>ff</sup> clAP2<sup>-/-</sup> mice were  
626 provided by Prof. W. Wei-Lynn Wong at the University of Zurich, Switzerland with the  
627 permission of Prof. John Silke, VIC Australia. RORyt<sup>CRE</sup> mice were provided by Prof.  
628 Gerard Eberl at Pasteur Institute, Paris, France. ROSA26-floxSTOPflox-RFP mice were  
629 from the Swiss Immunological Mouse Repository (SwImMR). Lymph nodes from  
630 TNFR1<sup>-/-</sup> mice were provided by Prof. William Agace at Lund University, Sweden, while  
631 Lymph nodes from clAP1<sup>UBA</sup> mutant mice were provided by Prof. Pascal Meier at The  
632 Institute of Cancer research, UK.

633 **Cell culture media and buffers**

634 For all preparations of single cell suspensions and cell cultures RPMI 1460 (Invitrogen)  
635 supplemented with 10% heat inactivated FBS (GIBCO), 20mM Hepes pH 7.4 (Gibco),  
636 50 µM 2-mercaptoethanol, 2 mM L-glutamine (Gibco) and 10,000 U/ mL penicillin-  
637 streptomycin (Gibco), was used. Where indicated, IMDM (Invitrogen) was used instead  
638 of RPMI 1460 and supplemented as aforementioned. FACS buffer was prepared by  
639 supplementing PBS with 3% heat inactivated FBS.

640 **Lymphocyte isolation from mouse organs**

641 Lymphocytes were isolated from peripheral lymph nodes (axial, brachial and inguinal),  
642 thymus, ear skin, small intestinal and colonic lamina propria following the previously  
643 described protocols (Kadekar *et al*, 2020). Lymphocytes were isolated from cervical and  
644 auricular lymph nodes in case of IMQ-induced psoriasis.

645 **Ex-vivo culturing of lymphocytes**

646 For staining of cytokines from lymphocytes that were isolated from peripheral lymph  
647 nodes of untreated mice, the cells were plated at a density of  $10 \times 10^6$  cells /ml in 1ml of  
648 supplemented RPMI in 12 well plates. The cells were restimulated with 50ng/ml PMA  
649 (phorbol myristate acetate; Sigma Aldrich), 750 ng/ml Ionomycin (Sigma Aldrich) and  
650 BD GolgiStop (containing monensin at 1:1000 dilution, BD) and cultured for 3.5 hours at  
651 37°C. For estimation of IL-22 production by CD4<sup>+</sup> and  $\gamma\delta^+$  T cells from homeostatic  
652 mice, the lymphocytes were first cultured overnight with 40ng/ml rmIL-23 (R&D) the  
653 restimulated with PMA, Ionomycin and BD GolgiStop as aforementioned. The cells  
654 were then harvested and used for flow cytometry staining.

655 In case of lymphocytes that were isolated from peripheral lymph nodes or skin in IMQ-  
656 experiments, the cells were plated at a density of  $5 \times 10^6$  cells /ml in 1ml of supplemented  
657 IMDM in 24 well plates. The cells were restimulated with 50ng/ml PMA (phorbol  
658 myristate acetate; Sigma Aldrich), 750 ng/ml Ionomycin (Sigma Aldrich) and BD  
659 GolgiPlug (containing Brefeldin A at 1:1000 dilution, BD) and cultured for 3.5 hours at  
660 37°C. The cells were then harvested and used for flow cytometry staining.

661 Alternatively, lymphocytes that were isolated from mesenteric lymph nodes or colonic  
662 lamina propria in *Citrobacter rodentium* infection experiments, the cells were plated at a  
663 density of  $5 \times 10^6$  cells /ml in 1ml of supplemented IMDM in 24 well plates. The cells were  
664 subsequently treated with 40ng/ml rmIL-23 (R&D) for 3 hours, followed by 50ng/ml PMA  
665 (phorbol myristate acetate; Sigma Aldrich), 750 ng/ml Ionomycin (Sigma Aldrich) and  
666 BD GolgiPlug (containing Brefeldin A at 1:1000 dilution, BD) and cultured for an  
667 additional 3.5 hours at 37°C.

668 For cell cycle assay experiments, lymphocytes that were isolated from peripheral lymph  
669 nodes of mice, were plated at a density of  $5 \times 10^6$  cells /ml in 1ml of supplemented RMPI

670 in 24 well plates. The cells were treated with either 20ng/ml rmIL-7 (R&D), or with 10  
671 ng/ml rmIL-1 $\beta$  (Biologen) + 20 ng/ml rmIL-23 (R&D), or 20 ng/ml rhIL-2 (Biologen), or  
672 anti-CD3 (2  $\mu$ g/ml; clone 145-2C11) for 48 hours. The cells were subsequently  
673 harvested for flow cytometry staining.

674 **IMQ-induced psoriasis**

675 Psoriasis was induced in mice by applying 7 mg of Aldara cream (containing 5%  
676 imiquimod) to the dorsal side of each ear for 7 days. Histological sections were  
677 prepared by fixing ear tissue in 10% formalin overnight and then paraffin embedded.  
678 The paraffin embedded sections were cut and stained by H&E.

679 **Flow cytometry staining**

680 Surface antigens, intracellular cytokines and cell cycle assay were stained for flow  
681 cytometry as previously described (Rizk *et al*, 2019). For transcription factor staining,  
682 the cells were first stained for live/dead discrimination followed by surface antigen  
683 staining and subsequently fixed using Foxp3 fixation/permeabilization buffer (Thermo  
684 Fisher) for 1 hour at 4°C. The cells were washed once with then stained with the desired  
685 antibodies in Foxp3 perm/wash buffer for 1 hour at 4°C. The cells were washed once  
686 again and resuspended in FACS buffer and analyzed using BD LSRFortessa.

687 The following antibodies were used herein at 1:200 dilution unless otherwise indicated:  
688 Fixed viability stain-700 (FVS700, BD, 1:1000), anti-IL-17A (TC11-18H10; BV786 and  
689 PE), anti-IFNy (XMG1.2; PE-Cy7, APC, BV711 and Percp-cy5.5), anti-IL-22  
690 (1H8PWSR; PE), anti-cMAF (symOF1; PE, eF660 or Percp-Cy5.5; 5  $\mu$ L/test), anti-CD4  
691 (GK1.5; BUV395 and FITC), anti-TCR $\gamma\delta$  (GL3; BV421 and APC), anti-KLRG1 ( 2F1 ,  
692 BV786), anti-CD27 (LG.3A10; PE-Cy7 and BV650), anti-CCR6 (140706; Alexa Fluor  
693 647), anti-CD44 (1M7; V500), anti-CD19 (6D5; FITC), anti-TCR $\beta$  (H57-597; APC-

694 eflour780), anti-CD3e (145-2C11, PeCF594 and PE), anti-Tbet(4B10; PeCy7), anti-  
695 CD8 (53-6.7;FITC), anti-V $\gamma$ 5 (536; FITC), anti-V $\gamma$ 4(UC3-10A6; Percp-eflour710), anti-  
696 GATA3(TWAJ; Percp-eFlour710; 1:30), anti-CD45(30-F11;PE and V500), anti-CD127  
697 (SB/199; BUV737) and anti-ROR $\gamma$ t (B2D; APC and PE).

698 **Administration of Anti-TNF**

699 For neutralization of TNF, 1 week old pups were weighed and i.p. injected with the a-  
700 TNF (Adalimumab, brand name HUMIRA) at 5 mg/kg body weight once a week until  
701 weaning. After weaning the mice were i.p. injected with 10 mg/kg body weight twice a  
702 week until euthanasia at approximately 12 weeks of age.

703 **Transfer of neonatal  $\gamma\delta$  T cells to RAG1 $^{-/-}$  hosts.**

704 First, thymi from 1-2 days old mice were isolated and crushed individually against 70  $\mu$ m  
705 filter to prepare single cell solutions. Subsequently, total  $\gamma\delta$  T cells were enriched by  
706 magnetic depletion of CD4 $^{+}$ , CD8 $^{+}$ , TCR $\beta$  $^{+}$  cells as follows: total thymocytes were re-  
707 suspended in MACS buffer at 1e8 cells/ml containing 50  $\mu$ L/ml normal rat serum and  
708 1:200 biotin labelled anti-CD4 $^{+}$  (GK1.5), CD8 $^{+}$  (53-6.7) and TCR $\beta$  $^{+}$  (H57-597)  
709 antibodies; the cells were incubated for 10 minutes at room temperature and then  
710 incubated with 75  $\mu$ L/ml EasySep RaphidSphere streptavidin beads (#50001) for 2.5  
711 minutes then transferred to EasySep magnet for 2.5 minutes. The non-bound fraction  
712 was collected by decantation and centrifugated for 5 minutes at 400g at 4°C.. The  
713 enriched  $\gamma\delta$  T cells from each donor mouse were re-suspended in PBS and then i.v.  
714 injected into the tail vein of a RAG1 $^{-/-}$  host. The RAG1 $^{-/-}$  hosts were euthanized for  
715 collection of organs after 12 weeks.

716 **Bone marrow chimeras**

717 The bone marrow cells for reconstitution were isolated by flushing the tibia and femur,  
718 which were dissected from donor mice, with culture media. Total bone marrow cells  
719 were then centrifuged at 400g for 5 minutes at 4°C. The cells were then re-suspended  
720 and passed through 70 µm filter. Subsequently, red blood cells were then lysed using  
721 RBC lysis buffer (Biolegend) and a single cell suspension of bone marrow cells was the  
722 prepared by passing the cells through 40 µm filter. The prepared cells were then  
723 counted and mixed as appropriate.

724 Conversely, host mice were sub-lethally irradiated by 2 doses of 4.5 Gy that were at  
725 least 4 hours apart. After 24 hours, the hosts were reconstituted with 10e6 bone marrow  
726 cells that were i.v. injected into the tail vein of the host mice. The hosts were euthanized  
727 for organs after at least 12 weeks.

## 728 **Immunofluorescent imaging of intestinal tissue**

729 To assess the presence of SILT in the intestines of WT or ΔIAP1/2 by confocal laser  
730 microscopy, the distal ileum was taken and flushed once with HBSS (Thermo Fisher) to  
731 remove intestinal contents. Cleaned intestines were fixed for 8h in 4% PFA (Sigma-  
732 Aldrich) in PBS and stored in washing buffer (PBS+5%FCS+0.2% Triton X-100 (Sigma-  
733 Aldrich)+0.01% Thimerosal (Sigma-Aldrich)) until further use. To prepare the collected  
734 intestines for staining, tissues were embedded in 4% UltraPure™ Low Melting Point  
735 Agarose (Thermo Fisher) in PBS, sectioned with a swinging blade microtome (Leica  
736 VT1200S) into 50 micron sections and permeabilized overnight using the Foxp3  
737 Transcription Factor Staining Buffer Set (Thermo Fisher). Permeabilized sections were  
738 stained in the supplied permbuffer with an antibody against RORyt (AFKJS-9;  
739 unconjugated), followed by a washing step in permbuffer and incubation with a  
740 biotinylated secondary antibody against the primary anti- RORyt antibody (Biotinylated

741 anti-rat; Jackson ImmunoResearch). To detect ROR $\gamma$ t<sup>+</sup> ILC and B cells, sections were  
742 washed again in permbuffer and incubated in permbuffer with antibody against B220  
743 (RA3-6B2; AF647) and streptavidin-conjugated AF555 (Thermo Fisher), as well as  
744 DAPI (Thermo Fisher) to stain all nucleated cells. Sections were washed one more time,  
745 mounted on glass slides with ProLong Gold (Thermo Fisher) and analyzed using an  
746 LSM710 confocal laser microscope (Carl Zeiss). Images of  $\geq 5$  different sections per  
747 mouse were acquired with the Zeiss Zen v2.3 software (Carl Zeiss) and analyzed using  
748 Imaris v8 (Bitplane/Oxford Instruments) and Fiji v2.1.0/1.53c (Schindelin *et al*, 2012).

749 **Murine *Citrobacter rodentium* infection**

750 Starter cultures of *Citrobacter rodentium* strain DBS100 (ATCC 51459; American Type  
751 Culture Collection) were grown overnight at 37°C in Luria-Bertani (LB) medium. The  
752 cultures were then used at 5% v/v to inoculate sterile LB medium. The cultures were  
753 grown at 37°C to an OD600 of 0.8- 1 and the CFU count was determined from the  
754 OD600 measurement using the following formula: CFU/ml =  $(5 \times 10^8)(OD) - 3 \times 10^7$ .  
755 Subsequently, the bacteria was collected by centrifugation at 4000g for 10 minutes. The  
756 bacterial pellet was then resuspended in LB medium to give at  $2 \times 10^9$  CFU/100  $\mu$ L. To  
757 infect adult mice, the mice were orally gavaged with either 100  $\mu$ L of *Citrobacter*  
758 *rodentium* or LB control. The mice were weighed before oral gavage and once daily until  
759 termination of the experiment. At day 12 post infection all mice were euthanized,  
760 dissected to collect organs and fecal samples.

761 The collected fecal samples were weighed and dissolved in PBS and then serially  
762 diluted. The serial dilutions were plated on Brilliance™ E. coli/coliform Agar (CM0956,  
763 Thermo Fisher) and incubated overnight at 37°C. *Citrobacter rodentium* colonies were  
764 identified as being pink colonies and enumerated, while E. coli colonies were identified

765 as purple colonies. CFU/g stool was then calculated as previously described  
766 (Bouladoux *et al*, 2017).

767 **Immunofluorescent imaging of nuclear RelB in  $\gamma\delta$  T cells**

768 Total lymphocytes were isolated from peripheral (axial, brachial and inguinal), cervical  
769 and auricular lymph nodes of 4 weeks old mice as described above. Subsequently, total  
770  $\gamma\delta$  T cells were enriched by magnetic depletion of CD4<sup>+</sup>, CD8<sup>+</sup>, CD19<sup>+</sup> and TCR $\beta$ <sup>+</sup> cells  
771 as aforementioned. The cells were then stained with FVS700 for discrimination of live  
772 and dead cells and then stained for surface antigens with the following antibodies: anti-  
773 TCR $\gamma\delta$  (GL3; APC), anti-CD27 (LG.3A10; PE-Cy7) and anti-TCR $\beta$  (H57-597; APC-  
774 eflour780) all at 1:200 dilution. The cells were subsequently sorted into TCR $\gamma\delta$ <sup>+</sup> CD27<sup>+</sup>  
775 or TCR $\gamma\delta$ <sup>+</sup> CD27<sup>-</sup> cells using BD ARIA-FUSION cell sorter. The sorted cells were  
776 collected into cell culture medium and centrifuged at 400g for 5 minutes at 4°C. The  
777 cells were then fixed using Foxp3 fixation/permeabilization buffer (Thermo Fisher) for 1  
778 hour at 4°C. The cells were washed once with then stained with Foxp3 perm/wash  
779 buffer containing anti-TCR $\gamma\delta$  (GL3; APC, 1:50), anti-CD3e (145-2C11 or 17A2; biotin,  
780 1:100) and anti-RelB (D-4, Santa-cruz, 1:40) for 1-hour 4°C in Foxp3 perm/wash buffer.  
781 Again, the cells were washed once and stained with streptavidin-conjugated AF488  
782 (Biolegend, 1:100) and anti-mouse AF555 (1:100) for 1 hour 4°C in Foxp3 perm/wash  
783 buffer. The cells were then washed once more as previous and stained with DAPI to  
784 highlight cell nuclei and washed once more with PBS. Washed cells were mounted on a  
785 glass slide using ProLong Gold and imaged with an LSM710 confocal laser microscope  
786 and were acquired and analyzed with the Zen v2.3 software and and Fiji v2.1.0/1.53c  
787 (Schindelin *et al*, 2012).

788 **Real-Time quantitative PCR**

789 At the indicated timepoints,  $\gamma\delta$  T cells were sorted from the thymus or lymph nodes of  
790 mice directly into RLT buffer mixed with  $\beta$ -mercaptoethanol. RNA was then extracted  
791 from using Qiagen RNAeasy microkit following the manufacturer's instructions.

792 Subsequently, cDNA was prepared using BioRad Iscript cDNA synthesis kit using the  
793 manufacturer's protocol. Gene expression was then measured by RT-qPCR reactions  
794 using BioRad SSOFast EvaGreen supermix, which were run on CFX96 (Biorad) and  
795 analyzed using Bio-rad CFX manager software. The following primers were used for  
796 RT-qPCR:

797 Actb, Fwd-GGCTGTATTCCCCTCCATCG, Rev- CCAGTTGGTAACAATGCCATGT;  
798 RelB, Fwd- GCTGGGAATTGACCCCTACA, Rev- CATGTCGACCTCCTGATGGTT;  
799 Birc2, Fwd- TGCCTGTGGTGGAACTGA, Rev- GCTCGGGTGAACAGGAACA.

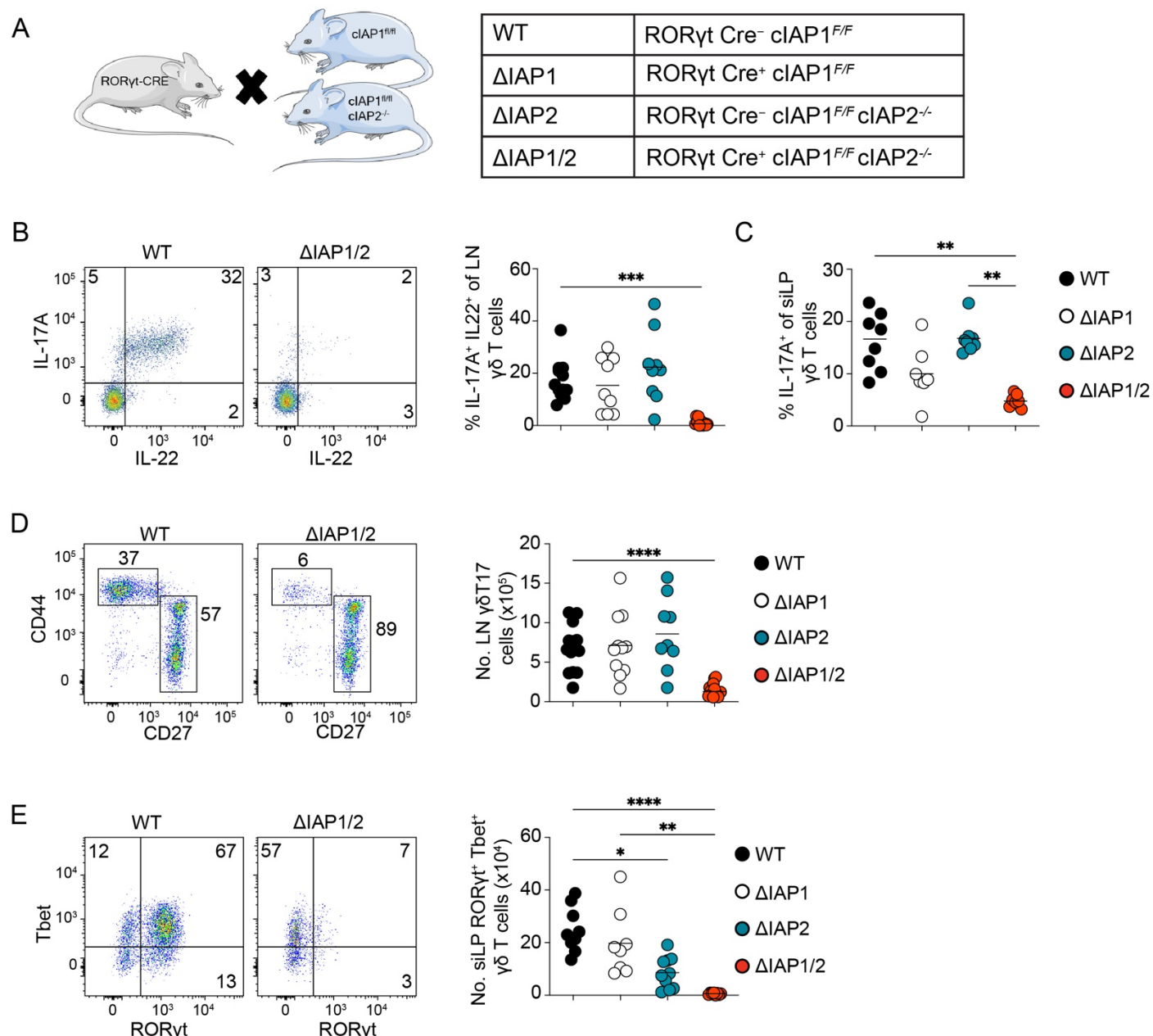
800

801

802

803 **Figures**

804 **Figure 1**



805

806 **Figure 1. clAP1 and clAP2 are required for the homeostasis of γδT17 cells in the**  
 807 **LNs and intestinal lamina propria.**

808 (A) Graphical representation of the different mouse strains generated by crossing  
 809 RORyt<sup>CRE</sup> mice to clAP1<sup>F/F</sup> or clAP1<sup>F/F</sup> clAP2<sup>-/-</sup> mice. Representative flow cytometric

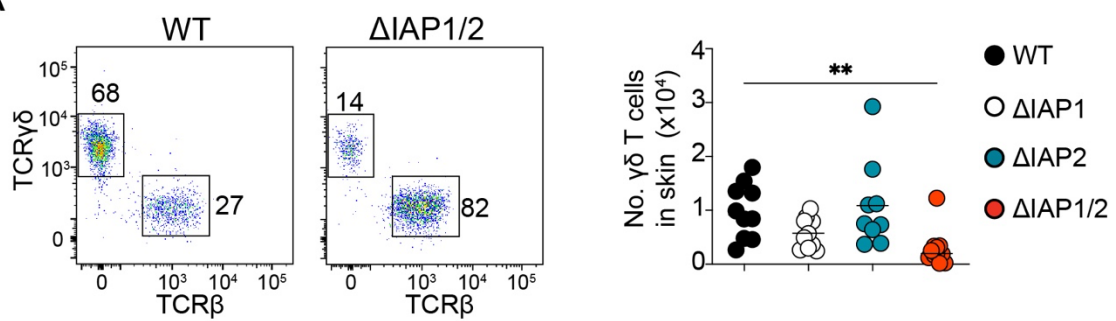
810 analysis (B) and frequency (B-C) of IL-17<sup>+</sup> IL-22<sup>+</sup> cells within  $\gamma\delta$  T cells in the LNs (B) or  
811 (C) IL-17<sup>+</sup> cells within  $\gamma\delta$  T in the siLP. (D) Representative flow cytometric analysis (dot  
812 plots) and numbers (graph) of  $\gamma\delta$ T17 cells in the LNs of adult WT,  $\Delta$ IAP1,  $\Delta$ IAP2 and  
813  $\Delta$ IAP1/2 mice. (E) Representative flow cytometric analysis (dot plots) and numbers  
814 (graph) of RORyt<sup>+</sup> Tbet<sup>+</sup>  $\gamma\delta$  T cells in the siLP of WT,  $\Delta$ IAP1,  $\Delta$ IAP2 and  $\Delta$ IAP1/2 mice.  
815 In graphs, each symbol represents a mouse, and lines represent the mean, data is pool  
816 of 4 experiments in (B) or 5 experiments in (C-E). \*P < 0.05, \*\*P < 0.01, \*\*\*P < 0.001,  
817 \*\*\*\*P < 0.0001 using Kruskal-Wallis test with Dunn's correction.

818

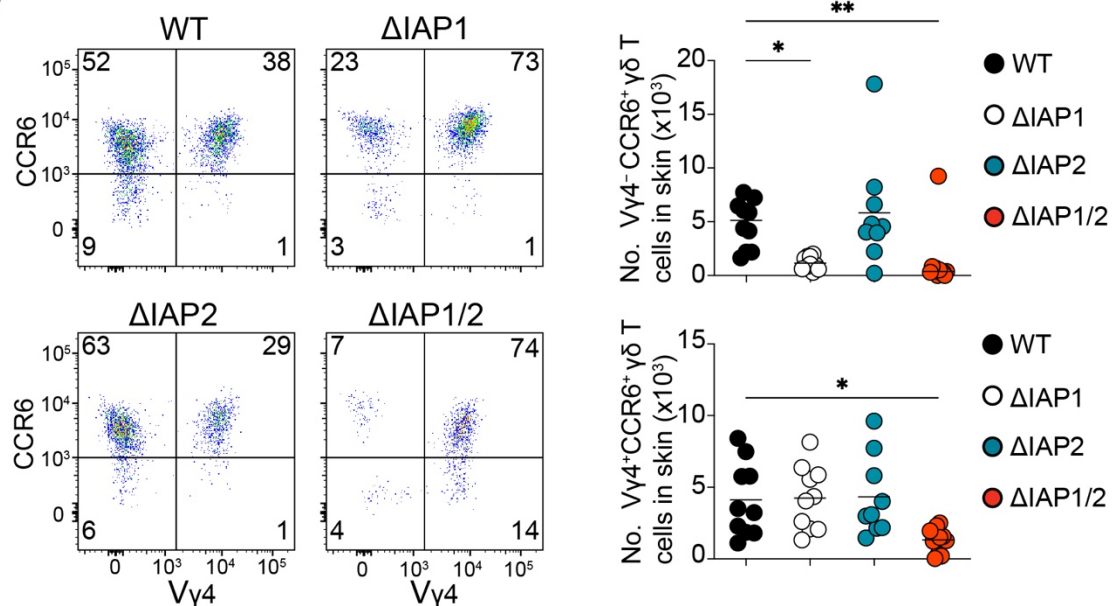
819

820 **Figure 2**

**A**



**B**



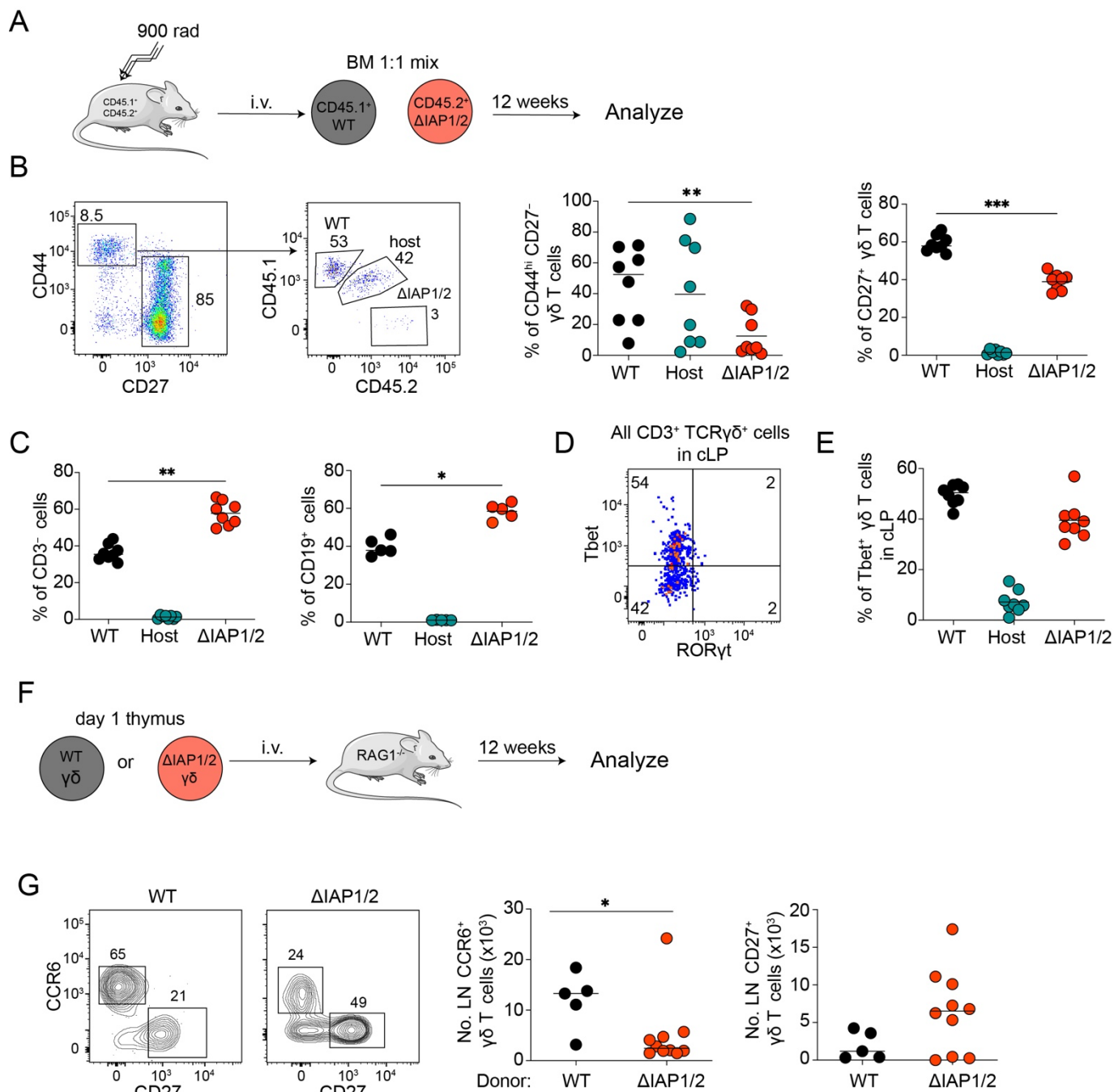
821

822 **Figure 2. cIAP1 and cIAP2 are non-redundantly required for the homeostatic  
823 maintenance of  $\gamma\delta$ T17 cell subsets in the skin.**

824 Representative flow cytometric analysis (dot plots) and numbers (graphs) of (A) total  $\gamma\delta$   
825 T cells or (B)  $V\gamma 4^+$  and  $V\gamma 4^-$  CCR6 $^+$   $\gamma\delta$  T cells in the skin of WT,  $\Delta$ IAP1,  $\Delta$ IAP2 and  
826  $\Delta$ IAP1/2 mice. In graphs, each symbol represents a mouse, and lines represent the  
827 mean, data is pool of 5 experiments in (A-B). \*P < 0.05, \*\*P < 0.01 using Kruskal-Wallis  
828 test with Dunn's correction.

829

830 **Figure 3**



831

832 **Figure 3. cIAP1 and cIAP2 are intrinsically required for the homeostasis of γδT17**  

833 **cells.**

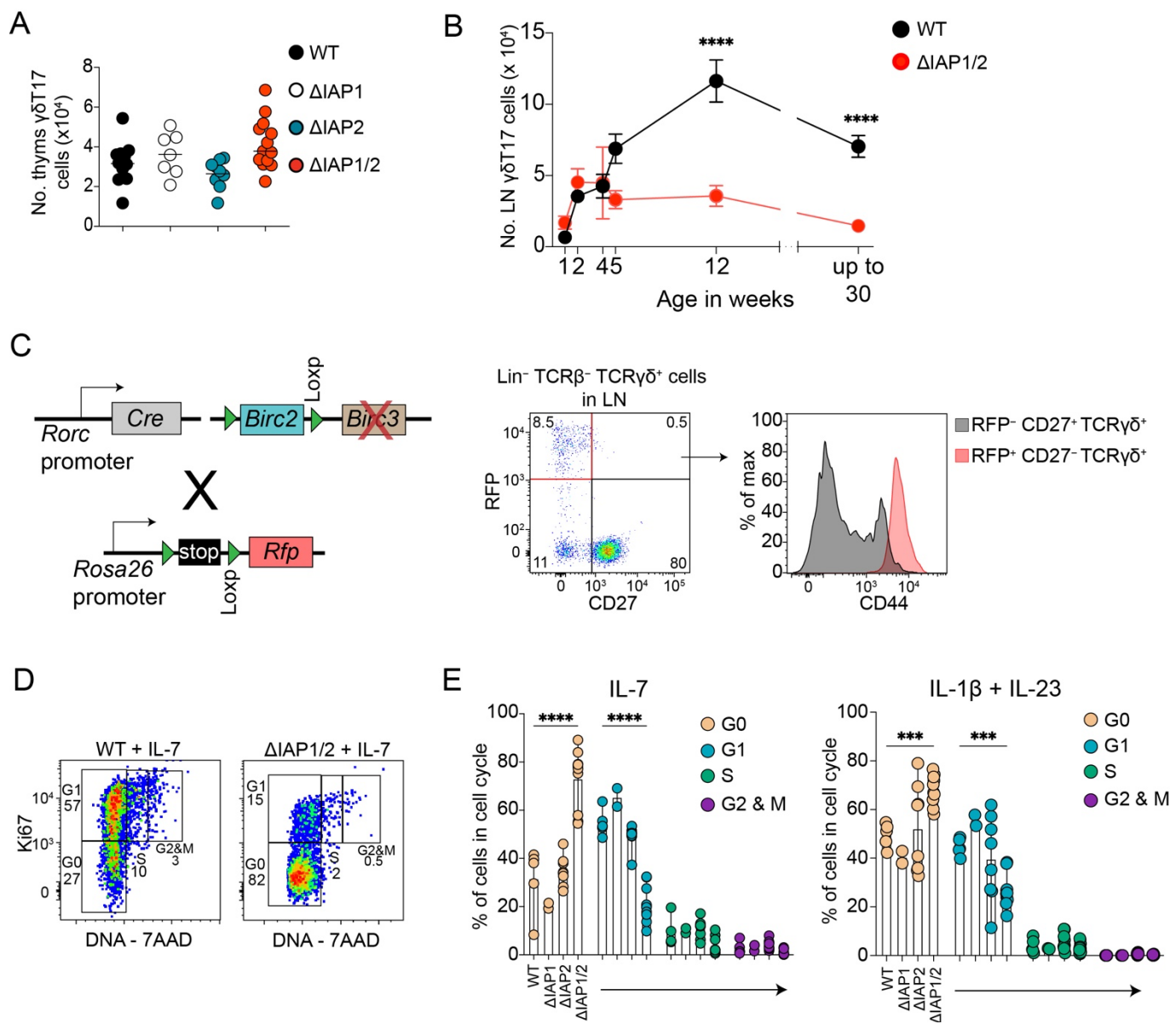
834 (A) Graphical representation of the experimental setup for competitive bone marrow  

835 experiments. (B) Representative flow cytometric analysis (dot plots) and frequency

836 (graphs) of WT (CD45.1<sup>+</sup>), host (CD45.1<sup>+</sup> CD45.2<sup>+</sup>) or ΔIAP1/2 (CD45.2<sup>+</sup>) -derived  
837 γδT17 and CD27<sup>+</sup> γδ T cells within γδ T cells population in the LNs of reconstituted  
838 hosts. (C) Frequency of WT (CD45.1<sup>+</sup>), host (CD45.1<sup>+</sup> CD45.2<sup>+</sup>) or ΔIAP1/2 (CD45.2<sup>+</sup>) -  
839 derived CD3<sup>-</sup> and CD19<sup>+</sup> cells in the LNs of reconstituted hosts. (D) Flow cytometric  
840 analysis and (E) frequency of RORyt<sup>+</sup> and Tbet<sup>+</sup> γδ T cells in the cLP of host mice  
841 following bone marrow reconstitution. (B-E) In graphs, each symbol represents a mouse,  
842 and lines represent the mean, data is pool of 3 experiments. \*P < 0.05, \*\*P < 0.01, \*\*\*P  
843 < 0.01 using one-way ANOVA with Tukey's correction. (F) Graphical representation of  
844 the experimental setup for transfer of neonatal γδ T cells to RAG1<sup>-/-</sup> recipients. (G) Flow  
845 cytometric analysis (contour plots) and numbers (graphs) of CCR6<sup>+</sup> CD27<sup>-</sup> or CD27<sup>+</sup> γδ  
846 T cells in the LNs of RAG1<sup>-/-</sup> hosts after transfer of neonatal γδ T cells from WT or  
847 ΔIAP1/2 pups. In graphs, each symbol represents a mouse, and lines represent the  
848 mean, data is pool of 3 experiments (G). \*P < 0.05 using Mann-Whitney test.

849

850 **Figure 4**



851

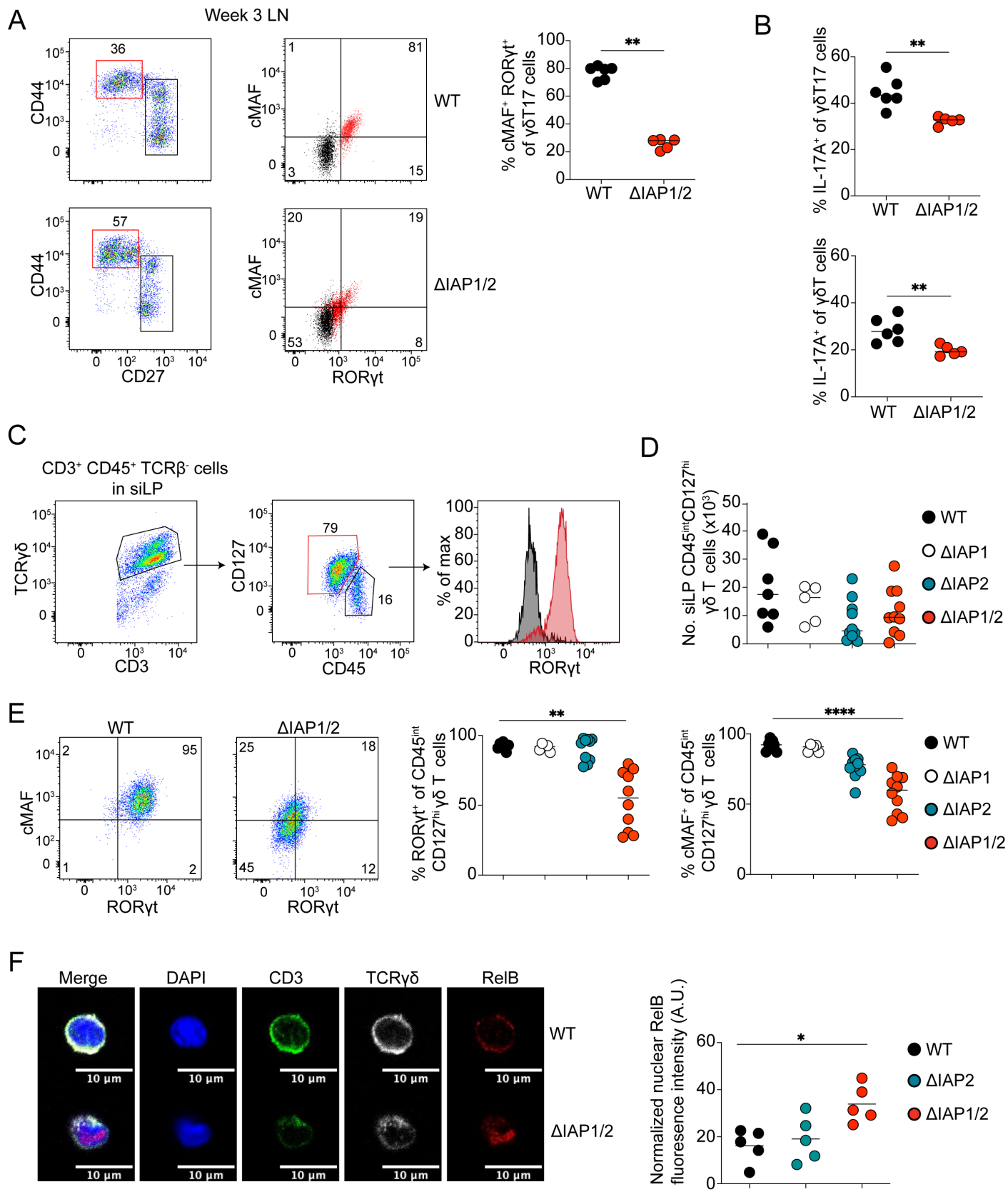
852 **Figure 4. cIAP1 and 2 double deficient  $\gamma\delta$ T17 cells are lost progressively during  
853 aging and fail to progress through cell cycle.**

854 (A) Numbers of  $\gamma\delta$ T17 cells in the thymi of 1-day old WT, ΔIAP1, ΔIAP2 and ΔIAP1/2  
855 pups. In graph, each symbol represents a mouse, and lines represent the mean, data is  
856 a pool of 3 experiments. (B) Numbers of  $\gamma\delta$ T17 cells in the LN of WT and ΔIAP1/2 at the  
857 indicated timepoints. Each symbol represents the mean amalgamated data from each  
858 timepoint and the error bars represents the SEM. \*\*\*\*P < 0.01 using Two-way ANOVA

859 with Holm-Sidak correction. (C) Graphical representation of the genetic makeup of the  
860  $\Delta$ IAP1/2 mice when crossed to the ROSA26-LSL-RFP strain, and representative flow  
861 cytometry analysis of LN  $\gamma\delta$ T17 cells from  $\Delta$ IAP1/2 x ROSA26-LSL-RFP mice. (D)  
862 Representative flow cytometric analysis and (E) frequency of cells in G0, G1, S or G2/M  
863 cell cycle stages within  $\gamma\delta$ T17 cells that were ex-vivo cultured with the indicated  
864 cytokines for 48 hours. In graphs, each symbol represents a mouse, and bars represent  
865 the mean, data is pool of 3 experiments. \*\*\*P < 0.001, \*\*\*\*P < 0.0001 using two-way  
866 ANOVA with Tukey's correction.

867

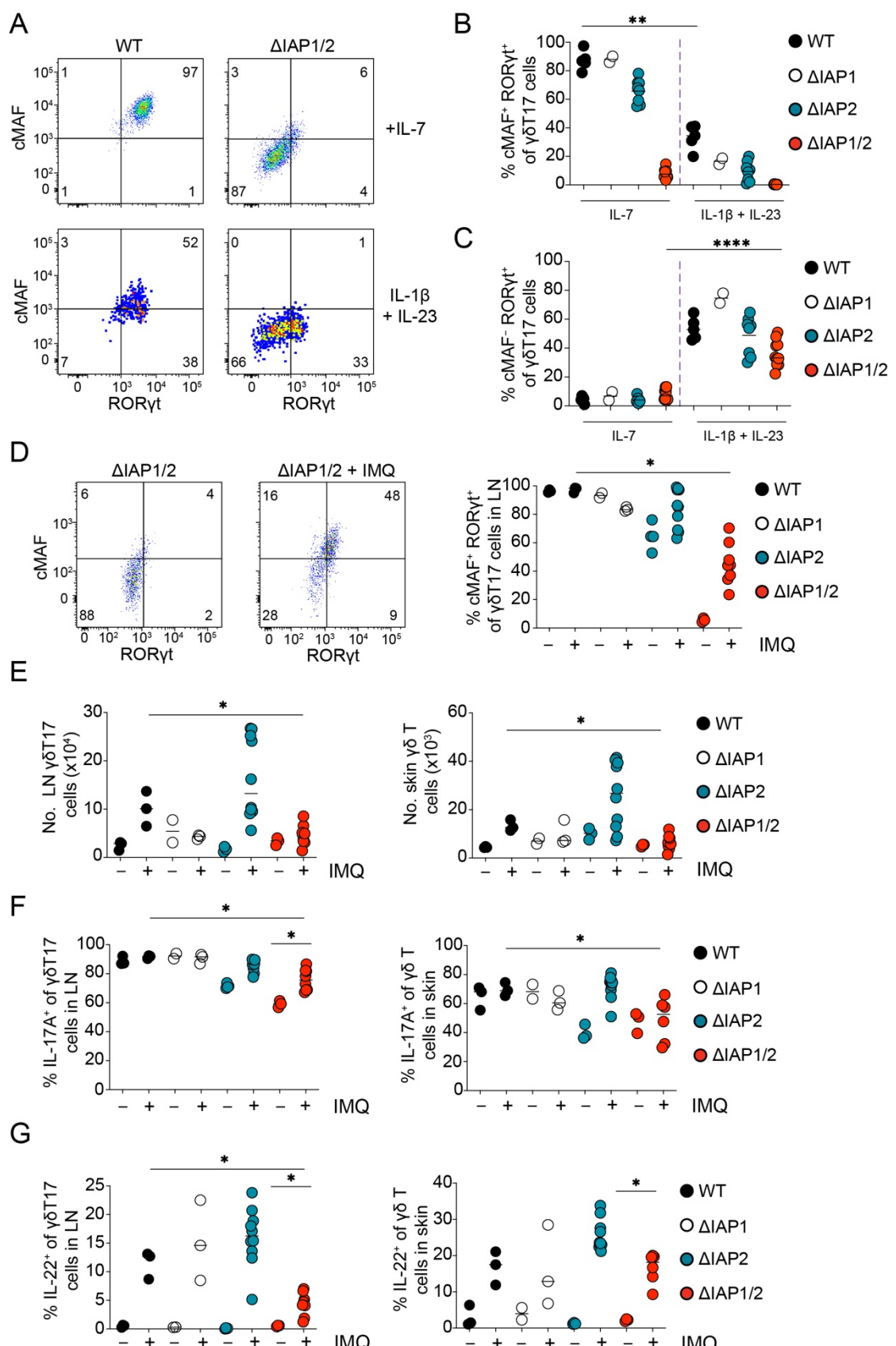
868 **Figure 5**



870 **Figure 5. cIAP1 and 2 maintain the transcription factor landscape of  $\gamma\delta$ T17 cells in**  
871 **the lymph nodes and intestinal lamina propria.**

872 (A) Flow cytometric analysis (dot plots) and frequency (graphs) of ROR $\gamma$ t<sup>+</sup> cMAF<sup>+</sup> cells  
873 within  $\gamma\delta$ T17 cells from the LNs of 3-week-old WT and  $\Delta$ IAP1/2 mice. (B) frequency of  
874 IL-17<sup>+</sup> cells within  $\gamma\delta$ T17 cells (top) or within all  $\gamma\delta$  T cells (bottom) from the LNs of 3-  
875 week-old WT and  $\Delta$ IAP1/2 mice. In graphs, each symbol represents a mouse, and the  
876 line represent the mean, data is pool of 2 experiments. \*\*P < 0.01 using Mann-Whitney  
877 test. (C) Flow cytometric analysis showing the gating strategy and expression of ROR $\gamma$ t  
878 by CD45<sup>int</sup> CD127<sup>+</sup>  $\gamma\delta$  T cells in siLP of adult WT mice. (D) Numbers of CD45<sup>int</sup> CD127<sup>+</sup>  
879  $\gamma\delta$  T cells in the siLP of 4-week-old WT,  $\Delta$ IAP1,  $\Delta$ IAP2 and  $\Delta$ IAP1/2 mice. (E) Flow  
880 cytometric analysis (dot plots) and quantification (graphs) of ROR $\gamma$ t or cMAF expression  
881 by CD45<sup>int</sup> CD127<sup>+</sup>  $\gamma\delta$  T cells in the siLP of 4-week-old WT,  $\Delta$ IAP1,  $\Delta$ IAP2 and  $\Delta$ IAP1/2  
882 mice. In graphs, each symbol represents a mouse, and the line represent the mean,  
883 data is pool of 4 experiments. (F) Representative immunofluorescent microscopy  
884 analysis of  $\gamma\delta$ T17 cells (CD27<sup>-</sup> TCR $\gamma\delta$ <sup>+</sup> cells) and normalized nuclear RelB fluorescence  
885 intensity in sorted from the LNs of 4-week-old WT or  $\Delta$ IAP1/2. Images are  
886 representative of four independent experiments. \*P < 0.05, \*\*P < 0.01, \*\*\*\*P < 0.001  
887 using using Kruskal-Wallis test with Dunn's correction.

888 **Figure 6**



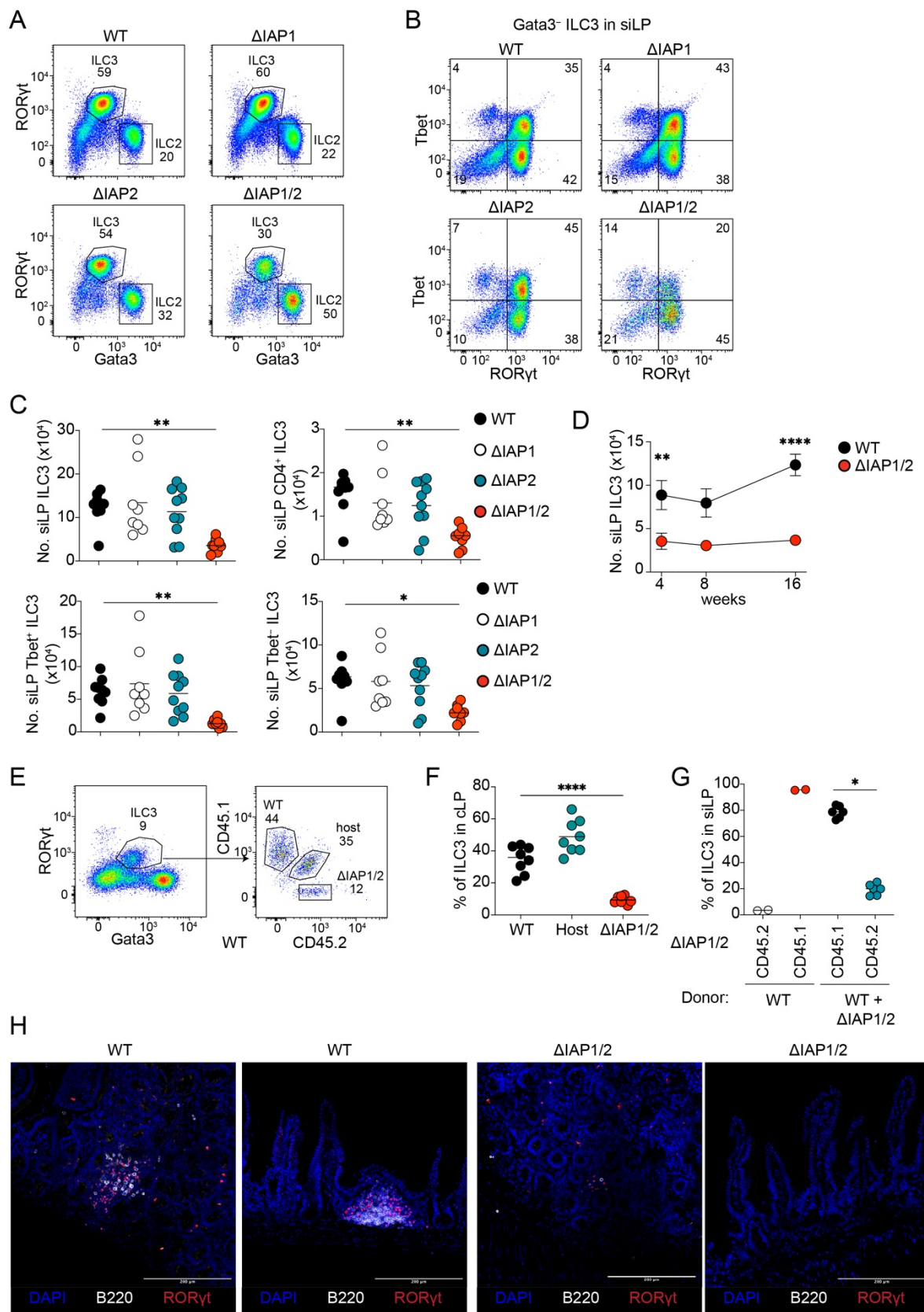
890 **Figure 6. Inflammation partially overcomes cIAP1 and cIAP2 deficiency in  $\gamma\delta$ T17  
891 cells.**

892 (A) Representative flow cytometric analysis and (B-C) quantification of ROR $\gamma$ t and  
893 cMAF expression by  $\gamma\delta$ T17 cells from the LNs of 4-week-old WT or  $\Delta$ IAP1/2 mice  
894 following ex-vivo culture with the indicated cytokines for 48 hours. In graphs, each  
895 symbol represents a mouse, and the line represent the mean, data is pool of 3  
896 experiments. (D) Representative flow cytometric analysis (dot plot) and quantification  
897 (graph) of ROR $\gamma$ t and cMAF expression by  $\gamma\delta$ T17 in LNs of 4-week-old control or IMQ-  
898 treated  $\Delta$ IAP1/2 mice. (E) Numbers of  $\gamma\delta$ T17 cells in the LNs (right) or skin (left) of 4-  
899 week-old control or IMQ-treated WT,  $\Delta$ IAP1,  $\Delta$ IAP2 or  $\Delta$ IAP1/2 mice. (F-G) Frequency  
900 of IL-17A $^+$  (F) or IL-22 $^+$  (G) cells within  $\gamma\delta$ T17 cells in the LNs or skin of 4-week-old  
901 control or IMQ-treated WT,  $\Delta$ IAP1,  $\Delta$ IAP2 or  $\Delta$ IAP1/2 mice. In graphs, each symbol  
902 represents a mouse, and the line represent the median, data is pool of 3 experiments.

903 \*P< 0.05, \*\*P < 0.01, \*\*\*\*P < 0.0001 using Mann-Whitney test.

904

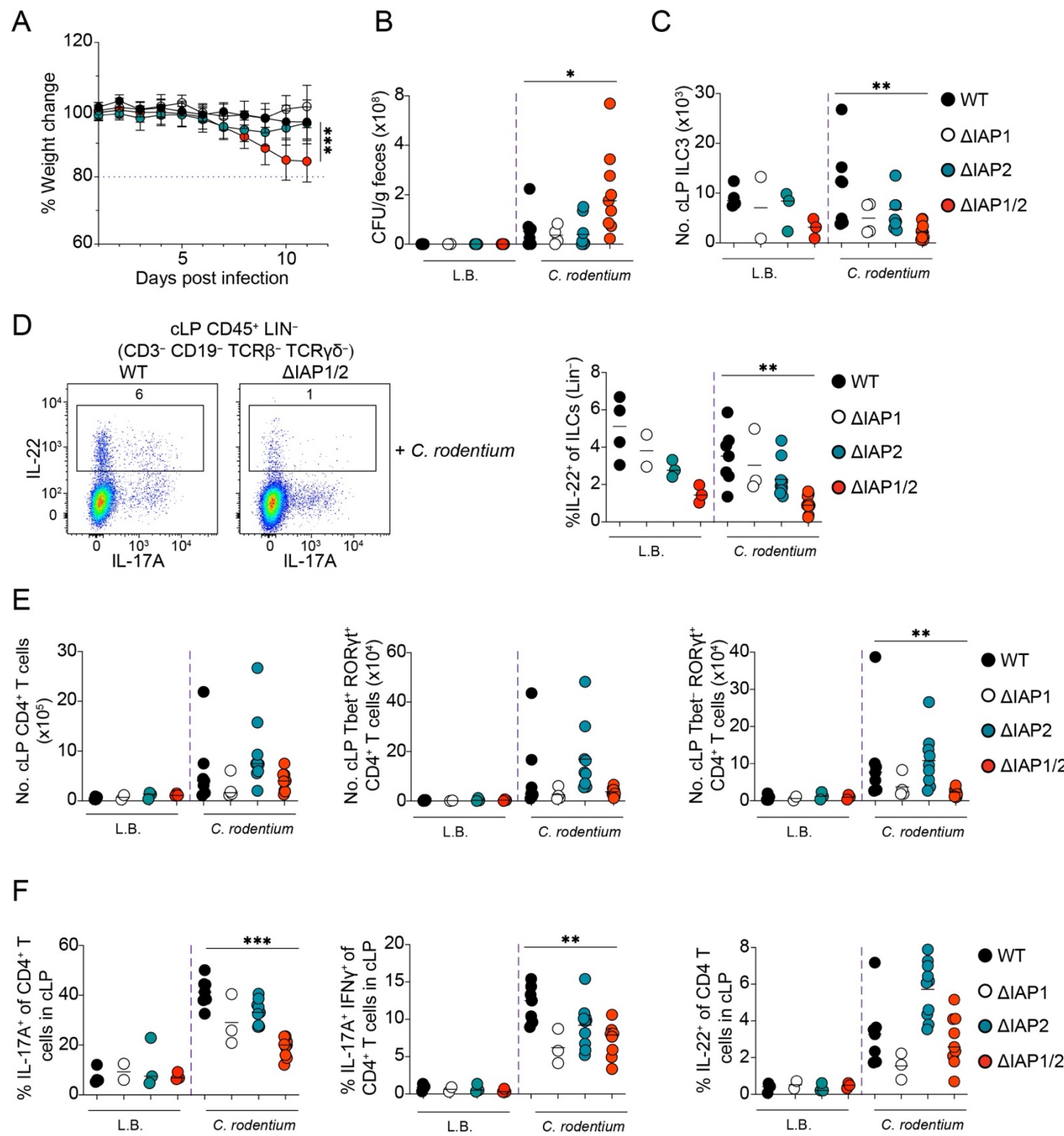
905 **Figure 7**



907 **Figure 7. cIAP1 and cIAP2 are intrinsically required for the maintenance of**  
908 **intestinal ILC3 and for ILF integrity**

909 Representative flow cytometric analysis of (A) total CD45<sup>+</sup> CD3<sup>-</sup> CD19<sup>-</sup> CD127<sup>+</sup> ILCs or  
910 (B) CD45<sup>+</sup> CD3<sup>-</sup> CD19<sup>-</sup> CD127<sup>+</sup> GATA3<sup>-</sup> cells in the siLP of adult WT, ΔIAP1, ΔIAP2 or  
911 ΔIAP1/2 mice. (C) Numbers of total ILC3s, CD4<sup>+</sup>, Tbet<sup>+</sup> or Tbet<sup>-</sup> ILC3s in the siLP of  
912 adult WT, ΔIAP1, ΔIAP2 or ΔIAP1/2 mice. In graphs, each symbol represents a mouse,  
913 and the line represent the mean, data is pool of 5 experiments. \*P< 0.05, \*\*P < 0.01  
914 using Kruskal-Wallis test with Dunn's correction. (D) Numbers of ILC3s in the siLP of  
915 WT and ΔIAP1/2 at the indicated timepoints. Each symbol represents the mean  
916 amalgamated data from each timepoint and the error bars represents the SEM. \*\*P <  
917 0.01, \*\*\*\*P < 0.0001 using Two-way ANOVA with Holm-Sidak correction.  
918 (E) representative flow cytometric analysis (dot plots) and (F) frequency (graph) of WT  
919 (CD45.1<sup>+</sup>), host (CD45.1<sup>+</sup> CD45.2<sup>+</sup>) or ΔIAP1/2 (CD45.2<sup>+</sup>)- derived ILC3 in the cLP of  
920 reconstituted hosts. In the graph, each symbol represents a mouse, and lines represent  
921 the mean, data is pool of 3 experiments. \*\*\*P < 0.01 using one-way ANOVA with  
922 Tukey's correction. (G) Frequency of WT (CD45.1<sup>+</sup>) or ΔIAP1/2(CD45.2<sup>+</sup>)- derived ILC3  
923 in the siLP of bone marrow reconstituted ΔIAP1/2 hosts. In graph, each symbol  
924 represents a mouse, and lines represent the mean, data is pool of 2 experiments. \*P <  
925 0.05 using Wilcoxon-rank t-test. (H) representative immunofluorescent microscopy  
926 images showing ILF structures in distal ileum sections from adult WT or ΔIAP1/2 mice.  
927 Images are representative of two independent experiments.

928 **Figure 8**



929

930 **Figure 8. RORyt<sup>Cre+</sup> cIAP1<sup>F/F</sup> cIAP2<sup>-/-</sup> succumb to *Citrobacter rodentium* infections.**

931 (A) Percentage body weight change of *C. rodentium* infected WT, ΔIAP1, ΔIAP2 and  
932 ΔIAP1/2 mice. Each symbol represents the mean amalgamated data from each

933 timepoint and the error bars represents the SD. \*\*\*P < 0.001 using Two-way ANOVA  
934 with Holm-Sidak correction. (B) Colony forming units (CFU) of *C. rodentium* in fecal  
935 matter of infected and uninfected WT,  $\Delta$ IAP1,  $\Delta$ IAP2 and  $\Delta$ IAP1/2 mice. (C) Numbers of  
936 ILC3s in the cLP of infected and uninfected mice. (D) representative flow cytometric  
937 analysis (dot blots) and frequency of IL-22 $^{+}$  cells within ILCs in the cLP of *C. rodentium*  
938 infected WT and  $\Delta$ IAP1/2 mice. (E) Numbers of total CD4 $^{+}$  T cells, Tbet $^{+}$  ROR $\gamma$ t $^{+}$  CD4 $^{+}$   
939 T cells, and ROR $\gamma$ t $^{+}$  Tbet- CD4 $^{+}$  T cells in the cLP of infected and uninfected mice. (F)  
940 Frequency of IL-17A $^{+}$ , IL-17A $^{+}$  IFN $\gamma$  $^{+}$  or IL-22 $^{+}$  cells within CD4 $^{+}$  T cells in the cLP of  
941 infected and uninfected mice. In graphs, each symbol represents a mouse, and lines  
942 represent the median, data is pool of 3 experiments. \*P < 0.05, \*\*P < 0.01, \*\*\*P < 0.001  
943 using Mann-Whitney test.